# *Reviews*

## Equiatomic Intermetallic Europium Compounds: Syntheses, Crystal Chemistry, Chemical Bonding, and Physical Properties

Rainer Pöttgen*

*Anorganisch-Chemisches Institut, Westfälische Wilhelms-Universität Münster, Wilhelm-Klemm-Strasse 8, D-48149 Münster, Germany*

Dirk Johrendt†

*Institut für Anorganische Chemie und Strukturchemie II, Heinrich-Heine-Universität Düsseldorf, Universitätsstrasse 1, (Geb. 26.42/26.32), D-40225 Düsseldorf, Germany*

*Received November 26, 1999. Revised Manuscript Received December 23, 1999*

The crystal chemistry of ternary equiatomic europium compounds EuTX (T = transition metal; X = element of the III, IV, or V main group) is reviewed. Besides preparation techniques we have especially focused on the structure−property relationships and peculiarities in chemical bonding. A main interest in these compounds is the valence state of the europium atoms. The magnetic susceptibility and electrical conductivity data, $^{151}$Eu Mössbauer spectroscopic results and $L_{III}$ X-ray absorption experiments are discussed in detail.

**Contents**



### 1. Introduction

Rare earth based intermetallic compounds have attracted considerable interest in recent years because of their greatly varying crystal structures and magnetic and electrical properties.[1−3] One large family within this huge number of intermetallics is represented by the equiatomic compounds RTX (R = rare earth or actinoid, T = transition metal, X = element of the p block) with more than 1000 representatives.[1] They crystallize with about 40 different structure types.[4]

Among these equiatomic compounds, those with cerium, europium, and ytterbium as rare earth component are possible candidates when screening for mixed valency; i.e., $Ce^{III}/Ce^{IV}$, $Eu^{II}/Eu^{III}$, and $Yb^{II}/Yb^{III}$. Here, the empty ($4f^0$), half filled ($4f^7$), and filled ($4f^{14}$) 4f shells of $Ce^{4+}$, $Eu^{2+}$, and $Yb^{2+}$, respectively, have a slightly enhanced stability. The corresponding cerium intermetallics have most intensively been investigated in the past when screening for new heavy fermion compounds. They display a large variety of different magnetic and electrical phenomena.[3,5]

Such cerium compounds are easily accessible by arc-melting of the elemental components. However, due to the low boiling points (high vapor pressure) of europium and ytterbium, such a simple synthesis is not possible for the intermetallic compounds EuTX and YbTX. This readily explains, why the corresponding europium and ytterbium compounds are frequently missing in the series of rare earth compounds.

By using modified preparative techniques, a whole series of such europium and ytterbium compounds is now accessible. Most of the europium compounds show divalent europium, while several ytterbium compounds exhibit mixed valency and/or phase transitions. First systematic investigations were carried out in the 1980s by the groups of Schuster and Mewis for a whole series of pnictides. More detailed investigations on the compounds with aluminum, gallium, indium, and the group IV elements were performed in the last five years.

In the present review, we focus on ternary equiatomic europium compounds EuTX and we report on their synthesis conditions and their crystal chemistry. Furthermore, we elucidate chemical bonding as well as group−subgroup relations which allow a comprehensive and compact explanation of the crystal chemical relationships. Also the various physical properties and spectroscopic measurements (magnetism, specific heat, Mössbauer spectroscopy, electrical conductivity, $L_{III}$ X-ray absorption spectra) are reviewed.

* E-mail: pottgen@uni-muenster.de.
† E-mail: johrendt@uni-duesseldorf.de.

10.1021/cm991183v CCC: $19.00 
Published on Web 03/24/2000

## 2. Syntheses

The preparations of the EuTX compounds mostly start directly from elemental components. Europium metal is used in the form of sublimed ingots, while the transition metals and main group elements are used in the form of wires, lumps, or powders (mainly for the platinum group metals). The use of larger lumps or ingots is highly recommended to minimize surface impurities. Powders with large surfaces may easily be oxidized, especially those of europium. Only the platinum metals can be used without a thought in powdered form.

The handling of europium is the main problem for the preparation of EuTX compounds. Surface impurities of EuO (NaCl type, ferromagnetic ordering at 70 K)[6,7] can irreversibly affect the magnetic measurements, already on the order of 0.5 wt %. Such EuO impurities in ternary samples manifest themselves by more or less large bumps in the $1/\chi$ vs $T$ plots as can often be seen in the literature. Large europium ingots should be cut in a drybox under an inert gas atmosphere in the absence of humidity. Commercial argon is most suitably purified over titanium sponge (900 K), molecular sieves, and an oxisorb catalyst.[8] Small pieces are best handled with the Schlenk technique.[9] Europium powders (too large and mostly oxidized surface) are as unsuitable as compact ingots with a large dark crust of oxidic and hydroxidic impurities. Contaminated europium can be purified via high vacuum distillation[10,11] to remove nonmetallic impurities, mostly dissolved gases.

Syntheses by arc-melting techniques are not appropriate for europium compounds since enormous weight losses occur due to the evaporation of europium metal even if very low currents (on the order of 10−20 A) and optimally water-cooled copper crucibles are used. To give an example: during an arc-melting synthesis of EuPtGe[12] europium boils (1870 K) before platinum melts (2040 K). This easily demonstrates that such an arc-melting procedure in quasi-open crucibles leads to uncontrolled reactions and causes problems with the correct composition of the samples.

These experimental problems can be overcome by reacting the elemental components in small alumina crucibles in sealed silica tubes under purified argon. By using this technique, samples of about 1000 mg can be prepared in single-phase form. By this way especially the EuTX pnictides were prepared.[13,14] Here, reactions in tantalum or niobium tubes may cause a significant side reaction of the pnictide component with the tube walls.

A very suitable method for all other compounds is the reaction of the elemental components in inert high-melting metal tubes, mainly niobium, tantalum, or molybdenum. The use of tantalum as container material was recently reviewed by Corbett.[15] The whole series of gallides, indium compounds, silicides, germanides, and stannides were prepared this way. The commercial tantalum tubes are usually cleaned with a mixture of $HNO_3$ (53%):HF (40%) = 1:1 followed by annealing at 1370 K in high vacuum. The elements are enclosed in tubes with typical volumes of 2 $cm^3$ in a miniaturized arc-melting apparatus.[16] The metal tubes were then sealed in evacuated silica tubes to prevent oxidation and the elemental components are reacted by heating at about 1300 K. Subsequently the temperature is lowered by a rate of 50 K/day and the tubes were held at temperatures between 770 and 1070 K for two more weeks. Alternatively, the sealed metal tubes can be heated under purified argon in a high-frequency furnace.[17] Both techniques allow preparations up to masses of about 2000 mg. No reactions of the samples with the tube materials were observed. All samples were routinely investigated by EDX analyses using a scanning electron microscope. Especially the annealing procedures in the high-frequency furnace result in very homogeneous samples.

Also glassy carbon is a very useful container material. The elemental components can be reacted under purified flowing argon in open glassy carbon crucibles in a high-frequency furnace. For this technique, a special, water-cooled reaction vessel with an observation window was constructed.[18] This setup allows very controllable reactions since the flux density can be augmented in very small steps. Another advantage is the direct observability of the reaction. The latter technique allows the preparation of samples with a total weight of about 1500 mg. Because of the controlled melting process, no evaporations and thus no weight losses occur during the reaction. This high-frequency technique is also useful for the growth of small single crystals for X-ray experiments.

## 3. Crystal Chemistry

In the following subchapters we list the equiatomic europium compounds EuTX in separate groups for the respective main group element as X component. Since aluminum and scandium have similar chemical behavior, we have also listed those compounds with T = aluminum. The lattice constants and the space groups are listed for all compounds emphasizing the crystal chemistry. For positional parameters of those compounds whose structures were refined from diffraction data, we refer to the original articles. Chemical bonding is discussed in detail in the fourth chapter and physical data of most compounds are reviewed in chapter 5.

**3.1. Equiatomic Aluminides EuTAl.** The aluminide EuAuAl[19] represents the so far only known equiatomic compound in the ternary systems europium−transition metal−aluminum. EuAuAl has been characterized on the basis of X-ray powder data. It crystallizes with a TiNiSi type structure,[20] space group *Pnma* (no. 62) with four formula units per cell. The lattice constants are $a$ = 754.29(8) pm, $b$ = 464.59(4) pm, $c$ = 773.45(7) pm, and $V$ = 0.27104(7) $nm^3$. The structure is built up from puckered $Au_3Al_3$ networks, derived from the $AlB_2$ structure. The occurrence of superstructure reflections (space group *Pnma*) indicates an ordering of the gold and aluminum atoms. A detailed description of TiNiSi type compounds is given in the following chapter.

**3.2. Equiatomic Gallides EuTGa.** The gallide EuAlGa[21] was characterized by X-ray powder data. It crystallizes with a $KHg_2$ type structure with a statistical distribution of the aluminum and gallium atoms on the mercury site. The X-ray data give no indication for long-range ordering. The $KHg_2$ type structure is discussed in detail in the next paragraph together with the transition metal gallides.

**Table 1. Lattice Constants and Residuals for EuTGa (T = Al, Cu, Zn, Rh, Pd, Ag, Pt, Au)**

| compd | type | *a* (pm) | *b* (pm) | *c* (pm) | *V*(nm$^3$) | *R* value | ref |
|---|---|---|---|---|---|---|---|
| EuAlGa | $KHg_2$ | 467.6 | 770.3 | 770.6 | 0.2776 | | 21 |
| EuCuGa | $KHg_2$ | 455.2(2) | 745.7(3) | 757.1(3) | 0.2570 | | 22 |
| EuZnGa | $KHg_2$ | 461.1(2) | 760.1(3) | 774.8(3) | 0.2716 | 0.041 | 25 |
| EuRhGa | PbFCl | 437.6(1) | = *a*[a] | 714.0(1) | 0.1366 | 0.025 | 28 |
| EuPdGa | TiNiSi | 729.2(2) | 449.2(1) | 784.1(2) | 0.2568 | | 22 |
| EuPdGa | TiNiSi | 730.30(7) | 451.13(4) | 780.66(7) | 0.2572 | 0.053 | 29 |
| EuAgGa | $KHg_2$ | 470.2(2) | 757.8(3) | 794.5(4) | 0.2831 | | 22 |
| EuAgGa | $KHg_2$ | 466.7(2) | 755.7(3) | 792.1(3) | 0.2794 | 0.124 | 24 |
| EuPtGa | TiNiSi | 730.4(3) | 446.2(2) | 770.7(3) | 0.2512 | | 22 |
| EuPtGa | TiNiSi | 727.6(1) | 447.1(1) | 768.2(1) | 0.2499 | 0.058 | 29 |
| EuAuGa | $KHg_2$ | 460.3(3) | 756.8(5) | 783.8(5) | 0.2730 | | 22 |
| EuAuGa | $KHg_2$ | 462.2(1) | 755.8(2) | 785.9(2) | 0.2745 | 0.067 | 24 |

[a] This value is equal to that given for the *a* constant.

The first investigations on the equiatomic europium transition metal gallides were carried out by Dwight in 1987.[22] He reported on EuCuGa, EuPdGa, EuAgGa, EuPtGa, and EuAuGa; however, these gallides were characterized only on the basis of X-ray powder data. Dwight assigned the $KHg_2$ type[23] structure (space group *Imma*) to EuCuGa, EuAgGa, and EuAuGa, while EuPdGa and EuPtGa were reported to crystallize with the ordered TiNiSi type[20] (space group *Pnma*). Structure refinements based on single-crystal X-ray data were performed recently.[24,25] These investigations confirmed the X-ray powder investigations of Dwight. Furthermore, the new gallide EuZnGa was synthesized. Lattice constants and residuals for these gallides are listed in Table 1.

It is worthwhile to note that the $KHg_2$ type structure[23] is frequently designated also as $CeCu_2$ type structure,[26] mainly in the physical literature. The $CeCu_2$ structure has been described in a setting which is different from that of the earlier reported $KHg_2$ structure. Parthé and Gelato have shown that the two structures are identical.[27] In the present review we consequently refer to the prototype $KHg_2$.

The structure refinements based on single-crystal data clearly showed that EuPdGa and EuPtGa crystallize with the TiNiSi type structure with an ordering of the palladium (platinum) and gallium atoms. Like EuAuAl (chapter 3.1), also these structures consist of puckered $Pd_3Ga_3$ and $Pt_3Ga_3$ networks. The europium atoms have a near-neighbor environment of two tilted and puckered hexagons, resulting in coordination number (CN) of 12. A perspective view of the EuPdGa structure is shown in Figure 1. Because of the puckering of the distorted hexagonal network, strong interlayer Pd−Ga interactions occur. This way each palladium atom has a distorted tetrahedral environment of gallium atoms and vice versa. A more detailed view of the TiNiSi type compounds is given in one of the next chapters together with the indium and tin compounds.

No long-range ordering of the transition metal and gallium atoms is evident from X-ray data of EuZnGa (Figure 2), EuAgGa, and EuAuGa. Neither powder nor single-crystal data revealed superstructure reflections which indicate an ordering between these atoms. However, the relatively short average transition metal−gallium distances within the distorted $T_3Ga_3$ networks indicate that a high degree of short range ordering exists. This is also expected from a crystal chemical point of view. Transition metal and gallium atoms

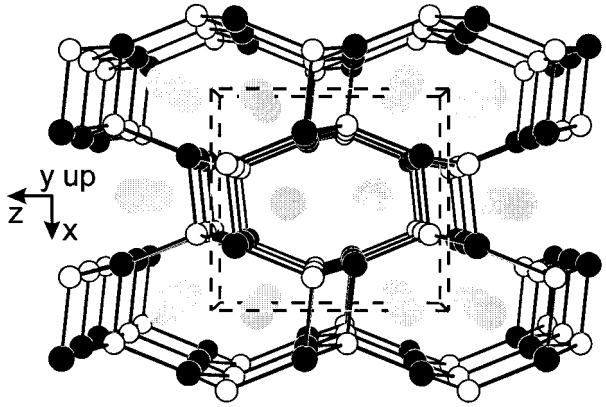


**Figure 1.** Perspective view of the EuPdGa structure. The three-dimensionally infinite [PdGa] polyanion is emphasized. The europium, transition metal (T), and gallium (X) atoms are drawn as large gray, filled, and open circles, respectively, throughout the paper.

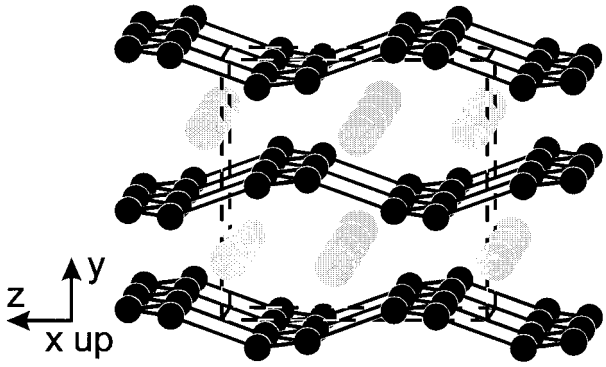


**Figure 2.** Perspective view of the EuZnGa structure. The three-dimensionally infinite [ZnGa] polyanion (small black circles) is emphasized.

statistically occupy the mercury position of the $KHg_2$ type. Refinements of the occupancy parameters always resulted in the expected compositions EuZnGa, EuAgGa, and EuAuGa.

EuRhGa[28] is the first gallide which adopts the PbFCl type structure (space group *P*4/*nmm*). Each rhodium atom has four gallium neighbors at 252 pm in a distorted tetrahedral environment (Figure 3). These $RhGa_{4/4}$ tetrahedra are linked via common edges, forming two-dimensionally infinite [RhGa] polyanions which are separated by the europium atoms. There are no close Rh−Rh and Ga−Ga contacts within these polyanions.

**3.3. Equiatomic Indium Compounds EuTIn.** The first indium compound reported in the literature was

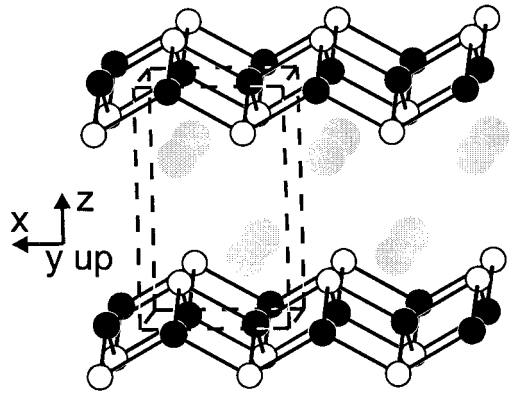


**Figure 3.** Crystal structure of EuRhGa. The two-dimensionally infinite [RhGa] polyanion is emphasized.

EuPdIn.[30,31] Ferro, Marrazza, and Rambaldi[30] discovered EuPdIn in 1974 during an investigation of the whole series of equiatomic RTIn compounds. On the basis of X-ray powder data, they assigned the $Fe_2P$ type structure to this europium compound (Table 2); however, some years later Cirafici and co-workers[31] showed that EuPdIn adopts the orthorhombic TiNiSi type structure, but they did not report the complete results for their structure refinement; especially the atomic displacement parameters were missing. The correct crystal structure was finally reported in 1996.[32] The main difference to the refinement of Cirafici et al. was the assignment of the correct Wyckoff sites to the palladium and indium atoms. It is clear now that EuPdIn adopts the TiNiSi type structure as EuPdGa does (Figure 1).

The palladium and indium atoms form a three-dimensional [PdIn] polyanion where each indium atom has four palladium neighbors at an average Pd−In distance of 283 pm, only slightly larger than the sum of Pauling's single bond radii[33] of 278 pm for palladium and indium. These short Pd−In distances indicate a considerable degree of covalent Pd−In bonding in the [PdIn] polyanion of EuPdIn. The palladium environment of the indium atoms resembles a distorted $PdIn_{4/4}$ tetrahedron. These tetrahedra are linked via common edges and corners, forming the three-dimensional polyanion in which the europium atoms are embedded (Figure 1). The pysical properties of EuPdIn are reviewed in chapter 5.

EuRhIn,[34] EuPtIn,[35] and EuAuIn[32] also crystallize with the TiNiSi type structure. The three structures have been refined on the basis of single-crystal X-ray data. They also consist of three-dimensional [RhIn], [PtIn], and [AuIn] polyanions, respectively, in which the europium atoms are embedded. The corresponding Rh−In, Pt−In, and Au−In distances agree well the sum of Pauling's single bond radii, indicating similar bonding characteristics as for EuPdIn.

EuZnIn[35] and EuAgIn[36] both crystallize with the $KHg_2$ type structure as isotypic EuZnGa does (Figure 2). While the silver compound has only been characterized from X-ray powder data, the structure of the zinc compound was refined from single-crystal data,[35] resulting in the composition $EuZn_{1.01(3)}In_{0.99(3)}$. The X-ray data of EuZnIn and EuAgIn gave no indication for long-range ordering of the transition metal and indium atoms. For both compounds no superstructure reflections indicating the TiNiSi type were observed. The average Zn−In and Ag−In distances of 281 pm and 287 pm, respectively, within the distorted hexagonal networks are only slightly longer than the sums of Pauling's single bond radii of 275 pm (Zn + In) and 284 pm (Ag + In). These relatively short distances certainly reflect a high degree of short-range order within the structures of EuZnIn and EuAgIn. Another important parameter which indicates a tendency via short-range order is the anisotropic displacement parameter $U_{22}$ of the statistically occupied Wyckoff site 8*h* of space group *Imma*. Most structure refinements of such equiatomic compounds with $KHg_2$ type structure show an at least two times larger parameter $U_{22}$ (as compared to $U_{11}$ and $U_{33}$). The $\pm y$ direction of the $KHg_2$ type compounds is the main displacement axis for the distortion of the polyanion in

**Table 2. Lattice Constants and Residuals for the Indium Compounds EuTIn (T = Zn, Rh, Pd, Ag, Pt, Au)**

| compd | type | *a* (pm) | *b* (pm) | *c* (pm) | *V* (nm$^3$) | *R* value | ref |
|---|---|---|---|---|---|---|---|
| EuZnIn | $KHg_2$ | 482.3(1) | 780.7(2) | 827.6(2) | 0.3116 | 0.0773 | 35 |
| EuRhIn | TiNiSi | 744.4(1) | 434.15(9) | 845.5(1) | 0.2733 | 0.0433 | 34 |
| EuPdIn | $Fe_2P$ | 830.9 | = *a*[a] | 395.7 | 0.2368 | | 30 |
| EuPdIn | TiNiSi | 747.4 | 446.4 | 852.9 | 0.2486 | | 31 |
| EuPdIn | TiNiSi | 748.30(13) | 447.20(8) | 853.50(14) | 0.2856 | 0.0408 | 32 |
| EuAgIn | $KHg_2$ | 492.7(2) | 784.3(2) | 845.5(3) | 0.3267 | 0.0789 | 36 |
| EuPtIn | TiNiSi | 746.94(8) | 447.27(6) | 843.46(9) | 0.2818 | 0.0689 | 35 |
| EuAuIn | TiNiSi | 755.2(2) | 472.2(1) | 842.3(2) | 0.3004 | 0.0470 | 32 |

[a] This value is equal to that given for the *a* constant.

**Table 3. Lattice Constants and Bragg Residuals (Rietveld Data) for the Silicides EuTSi (T = Al, Mg, Zn, Pd, Ag, Pt)**

| compd | type | *a* (pm) | *b* (pm) | *c* (pm) | *V* (nm$^3$) | *R* value | ref(s) |
|---|---|---|---|---|---|---|---|
| EuAlSi | $AlB_2$ | 415.5 | = *a*[a] | 451.0 | 0.0679 | | 37 |
| EuMgSi | TiNiSi | 771.3(2) | 455.5(1) | 836.6(3) | 0.2939 | | 39 |
| EuZnSi | ZrBeSi | 430.2(1) | = *a* | 861.6(3) | 0.1381 | | 38 |
| EuPdSi | LaIrSi | 641.9(1) | = *a* | = *a* | 0.2645 | 0.0251 | 40, 44 |
| EuPdSi | LaIrSi | 642.8 | = *a* | = *a* | 0.2656 | | 41 |
| $EuPd_{0.56}Si_{1.44}$[b] | $AlB_2$ | 416.1(1) | = *a* | 433.5(1) | 0.0650 | 0.0176 | 44 |
| $EuPd_{1.33}Si_{0.67}$[b] | $MgZn_2$ | 556.2(1) | = *a* | 907.0(1) | 0.2430 | 0.0493 | 44 |
| EuAgSi | $AlB_2$ | 420.3 | = *a* | 446.5 | 0.0683 | | 42 |
| EuPtSi | LaIrSi | 643.6 | = *a* | = *a* | 0.2666 | | 41 |
| EuPtSi | LaIrSi | 642.0(5) | = *a* | = *a* | 0.2646 | 0.0423 | 43, 44 |

[a] These values are equal to those given for the *a* constant. [b] High-pressure products of EuPdSi.

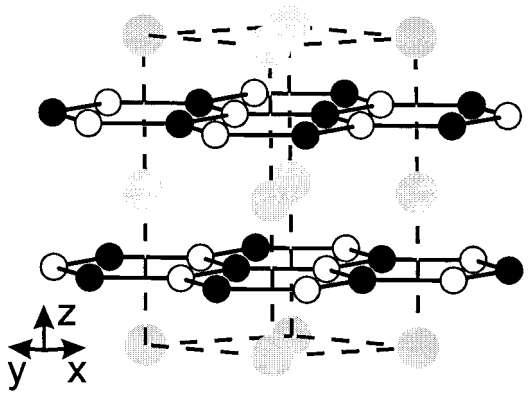


**Figure 4.** Crystal structure of hexagonal EuZnSi. The two-dimensionally infinite [ZnSi] polyanion is emphasized.

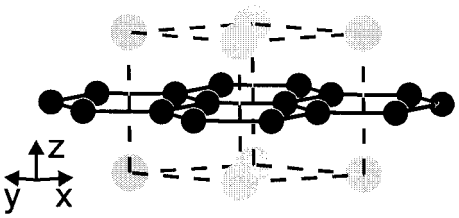


**Figure 5.** Crystal structure of hexagonal EuAgSi with $AlB_2$ type structure. The two-dimensional [AgSi] polyanion is emphasized.

going to the TiNiSi type (superstructure of the $KHg_2$ type). This was discussed in detail in reference.[35]

Although a large number of indium compounds has been synthesized, no equiatomic compounds with the higher homologue thallium are known until now.

**3.4. Equiatomic Silides EuTSi.** Six equiatomic silicides are known (Table 3). EuAlSi[37] adopts the simple $AlB_2$ type structure (Figure 5). The aluminum and silicon atoms randomly occupy the boron site. The ordering was not studied. With divalent magnesium and zinc, the Zintl phases EuMgSi and EuZnSi have been reported;[38,39] however, they have only been characterized on the basis of X-ray powder data. EuMgSi adopts the TiNiSi type structure (Figure 1) and EuZnSi (Figure 4) crystallizes with the ZrBeSi type (space group $P6_3/mmc$), a ternary ordered variant of $AlB_2$. Both structures are built up from ordered $Mg_3Si_3$ and $Zn_3Si_3$ hexagons, which are puckered in EuMgSi and planar in EuZnSi. According to the "$8 - N$" rule, the formulae of these silicides may be written as $Eu^{2+}Mg^{2+}Si^{4-}$ and $Eu^{2+}Zn^{2+}Si^{4-}$. There are consequently eight valence electrons within the two-dimensionally infinite $[MgSi]^{2-}$ and $[ZnSi]^{2-}$ polyanions. Since the ZrBeSi type structure of EuZnSi has only fixed parameters, the Zn−Si distance of 248 pm can be calculated from the lattice constants. The Zn−Si distance is only slightly larger than the sum of Pauling's single bond radii[33] of 242 pm for zinc and silicon, indicating a considerable degree of covalent Zn−Si bonding within the heterographite [ZnSi] network.

EuAgSi[42] (Figure 5) adopts the simple structure of $AlB_2$ (space group $P6/mmm$). The X-ray powder investigation revealed no long-range ordering between the silver and silicon atoms on the boron position. The average Ag−Si distance calculated from the lattice constants amounts to 243 pm, significantly shorter than the sum of Pauling's single bond radii[33] of 251 pm for silver and silicon. This reduced distance, however, is a clear indication for a high degree of short-range order within the two-dimensional [AgSi] polyanion. Similar Ag−Si distances have recently also been observed in the structures of $Ca_4Ag_2[Si_6]$, $Ba_4Ag_2[Si_6]$, and $Eu_4Ag_2[Si_6]$: 246−259 pm.[45]

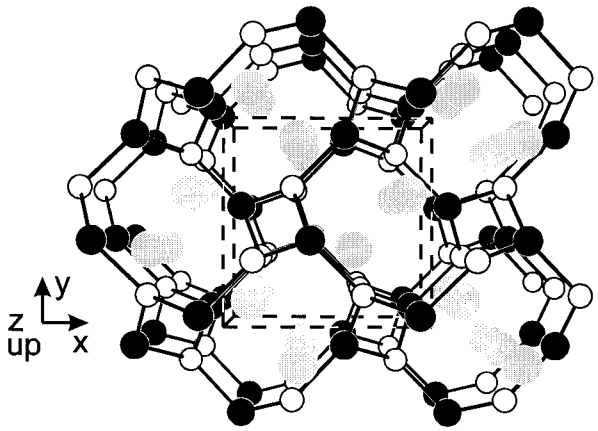


**Figure 6.** Crystal structure of cubic EuPdSi with LaIrSi type structure. The three-dimensional [PdSi] polyanion is outlined.

EuPdSi[40,41] and EuPtSi[41,43] both adopt the noncentrosymmetric cubic LaIrSi structure[46] (space group $P2_13$), a ternary ordered variant of the $SrSi_2$ type (space group $P4_132$).[47−49] Since space group $P2_13$ is a "translationengleiche" subgroup (t2) of $P4_132$, the ordering between the transition metal and silicon atoms expresses itself only in a change of the subcell intensities. As outlined in Figure 6, the palladium (platinum) and silicon atoms built up a three-dimensionally infinite [PdSi], respectively [PtSi] polyanion in which the divalent europium atoms are embedded. Within the polyanions, each palladium (platinum) atom has three silicon neighbors and vice versa. The corresponding Pd−Si and Pt−Si distances amount to 232 and 233 pm,[40,43,44] significantly shorter than the sums of the metallic single bond radii[33] of 246 pm (Pd + Si) and 247 pm (Pt + Si), respectively, indicating strong covalent bonding within both polyanions. A very wide and comprehensive description of these LaIrSi type silicides was given by Evers and co-workers.[40,43]

The structure of EuPdSi was studied also under high-pressure conditions.[44] At 4 GPa and 1120 K the cubic normal pressure (NP) phase transforms to a mixture of about 20% silicon-rich $EuPd_{0.56(2)}Si_{1.44(2)}$ with $AlB_2$ type structure (Figure 5) and about 80% of palladium-rich $EuPd_{1.33(1)}Si_{0.67(1)}$ with $MgZn_2$ type structure (space group $P6_3/mmc$) as shown in Figure 7. In both high-pressure (HP) phases, the density is higher than in the NP-phase. The shortest Pd−Si distance of 231 pm in HP-$EuPd_{1.33(1)}Si_{0.67(1)}$ is comparable to the NP-phase, while this distance is increased to 240(2) pm in HP-$EuPd_{0.56(2)}Si_{1.44(2)}$ with $AlB_2$ structure.

**3.5. Equiatomic Germanides EuTGe.** The equiatomic germanides EuTGe exhibit an unusually large structural variety. The 11 germanides listed in Table 4 crystallize with nine different structure types. The Zintl phases EuMgGe[39] and EuCdGe[38] both crystallize with the TiNiSi type structure (see Figure 1) in space group $Pnma$. The formulae of these germanides may to a first approximation be written as $Eu^{2+}Mg^{2+}Ge^{4-}$ and $Eu^{2+}Cd^{2+}Ge^{4-}$ with eight valence electrons within the

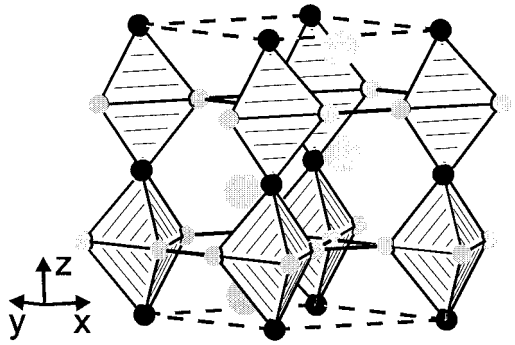


**Figure 7.** Crystal structure of HP-$EuPd_{1.33}Si_{0.67}$ with hexagonal $MgZn_2$ type structure. The three-dimensional [$Pd_{1.33}Si_{0.67}$] polyanion is outlined. The small gray circles within the polyanion indicate mixed palladium−silicon occupancy.

slightly puckered $[MgGe]^{2-}$ and $[CdGe]^{2-}$ polyanions. Because of the powder investigations no precise atomic parameters (and thus the degree of puckering within the polyanions) are available.

EuAlGe[50] was characterized on the basis of Guinier powder data. These investigations showed a tetragonal unit cell resembling the α-$ThSi_2$ type structure.[51] The ordering of aluminum and germanium on the silicon site of the α-$ThSi_2$ structure was not studied. An ordered substitution variant of the α-$ThSi_2$ structure (space group $I4_1/amd$) is the LaPtSi type (space group $I4_1md$).[52] Since $I4_1md$ is a "translationengleiche" subgroup of index 2 (t2) of $I4_1/amd$, the ordering between aluminum and germanium changes only the subcell intensities. Precise single-crystal data for EuAlGe are desirable to investigate the ordering. A perspective view of the EuAlGe structure is given in Figure 8, assuming the ordering variant of the LaPtSi type. The aluminum and germanium atoms have a nearly trigonal planar coordination of each other, forming a three-dimensional [AlGe] network, in which the europium atoms are embedded.

EuScGe[53] crystallizes with a ternary ordered version of the $La_2Sb$ type structure (space group $I4/mmm$).[63] The $La_2Sb$ type may itself be described as a vacancy derivative of the well-known $K_2NiF_4$ structure according to $Eu_2\square(Sc_2Ge_2) \equiv K_2NiF_4$. The EuScGe structure is drawn in Figure 9 with the refined atomic parameters of isotypic CeScGe.[53] The structure consists of distorted fcc-like slabs which resemble the $CeMg_2Si_2$ type.[61] The nickel position of the $K_2NiF_4$ structure remains empty, and the germanium atoms dislocate from the europium plane, leading to slightly compressed $Sc_4Ge_2$ octahedra (Sc−Ge 287 pm; Sc−Sc 302 pm). Chemical bonding in EuScGe is very interesting. The europium atoms as the most electropositive component of EuScGe transfer their two valence electrons (the divalent character of europium in EuScGe was determined from $L_{III}$ spectra)[64] to the network of compressed and condensed (via the scandium edges) $Sc_4Ge_2$ octahedra, leading to a formula $Eu^{2+}[ScGe]^{2-}$. Since the isolated germanium atoms tend to reach the octet ($Ge^{4-}$, $4s^24p^6$), the surplus electron of scandium is most likely involved in Sc−Sc bonding. This may already be inferred from the Sc−Sc distances (302 pm) which are significantly smaller than in hcp scandium (average Sc−Sc distance of 328 pm).[65] Chemical bonding in EuScGe is discussed in detail in chapter 5 on the basis of electronic structure calculations.

EuNiGe[54] and EuPdGe[44,58] crystallize with a common structure type (space group $P2_1/n$) which was first reported for the nickel germanide. They can be described as a strongly distorted, ordered derivative of the $CoSb_2$ type.[66] So far this structure type has only been reported for these two europium compounds, for CaPdSi[40] and for LaNiGa.[67] The palladium and germanium atoms in EuPdGe both have three germanium, respectively palladium neighbors. They form two-dimensionally infinite [PdGe] polyanions which consist of corrugated $4.8^2$ nets as outlined in Figure 10. These polyanions are strongly folded up, and the resulting polyanionic packages (Figure 11) are separated by the europium atoms. The average Pd−Ge distance in the polyanion of 248 pm is close to the sum of the metallic radii[33] of 251 pm, indicating strong covalent Pd−Ge bonding. Additionally some weak Pd−Pd interactions exist although the Pd−Pd distance of 289 pm is longer than in fcc palladium[65] where each palladium atom has 12 nearest palladium neighbors at 275 pm.

At 4 GPa and 1270 K, NP-EuPdGe transforms to HP-EuPdGe[44] with TiNiSi type structure (Figure 1). Because of the pressure-induced phase transition, each palladium atom has now four germanium neighbors in the HP modification. As expected from the pressure−distance paradoxon, the average Pd−Ge distance of 266 pm in HP-EuPdGe is significantly larger than in NP-EuPdGe (248 pm).

EuCuGe was first investigated by Iandelli on the basis of X-ray powder data.[56] Iandelli could index the powder patterns with an orthorhombic unit cell, similar to that of CaCuGe[18,68,69] (space group $Pnma$), however, only a moderate agreement with the calulated intensities (assuming the positional parameters of CaCuGe) was observed. We have recently investigated independently powders and single crystals of EuCuGe.[55] Several samples were compatible with the $AlB_2$ type structure (Figure 5) with the lattice constants listed in Table 4. The structure refinement[70] based on single-crystal X-ray data resulted in a composition $EuCu_{0.95(8)}Ge_{1.05(8)}$ with a statistical occupancy of the boron site by copper and germanium ($AlB_2$ type, space group $P6/mmm$). The single-crystal data gave no indication for long-range ordering between copper and germanium. The lattice constants of this (and other) single crystals were in good agreement with the Guinier powder data. The anisotropic displacement parameters gave no indication for a puckering of the planar polyanion. The CaCuGe type has 12 formula units per cell; however, only a factor of 10.9 was observed between the cell volume of the small $AlB_2$ type cell and the cell proposed by Iandelli. This inconsistency may be indicative of a difference in composition for the two samples. Further investigations on the whole series $EuCu_{2-x}Ge_x$ from $EuCu_2$ to EuCuGe are desirable to determine the structures and the homogeneity ranges.

In contrast to EuCuGe, EuZnGe crystallizes exhibiting a fully ordered structure. This germanide was first investigated by Merlo et al.[38] by X-ray powder data. They correctly assumed the ZrBeSi type (Figure 4, space group $P6_3/mmc$). This was confirmed later by a single-crystal investigation.[57] The structure consists of ordered, planar $Zn_3Ge_3$ hexagons which are rotated by 60 ° in every other layer. EuZnGe is a Zintl phase according to

**Table 4. Lattice Constants and Residuals for the Germanides EuTGe (T = Mg, Al, Sc, Ni, Cu, Zn, Pd, Ag, Cd, Pt, Au)**

| compd | type | *a* (pm) | *b* (pm) | *c* (pm) | $\beta/\gamma$ (deg) | *V* (nm$^3$) | *R* value | ref(s) |
|---|---|---|---|---|---|---|---|---|
| EuMgGe | TiNiSi | 775.6(2) | 458.0(1) | 844.4(2) | | 0.3000 | | 39 |
| EuAlGe | α-$ThSi_2$ | 420.0(1) | = *a*[a] | 1460.4(6) | | 0.2576 | | 50 |
| EuScGe | $La_2Sb$ | 427.0(1) | = *a* | 1563.6(8) | | 0.2851 | | 53 |
| EuNiGe | EuNiGe | 699.6(1) | 758.1(1) | 618.7(1) | 130.22 ($\gamma$) | 0.2506 | 0.052 | 54 |
| EuCuGe | $AlB_2$ | 422.09(8) | = *a* | 441.61(8) | | 0.0681 | 0.0309 | 55 |
| EuCuGe | CaCuGe | 2209(1) | 754.3(5) | 445.3(2) | | 0.7420 | | 56 |
| EuZnGe | ZrBeSi | 435.7(1) | = *a* | 862.1(1) | | 0.1417 | | 38 |
| EuZnGe | ZrBeSi | 437.2(1) | = *a* | 860.4(2) | | 0.1424 | 0.0297 | 57 |
| EuPdGe | EuNiGe | 617.9(1) | 612.0(1) | 742.7(1) | 109.48 ($\beta$) | 0.2648 | 0.0364[b] | 44 |
| EuPdGe | EuNiGe | 618.1(1) | 613.6(1) | 743.9(1) | 109.40 ($\beta$) | 0.2661 | 0.0536 | 58 |
| HP-EuPdGe | TiNiSi | 737.6(1) | 447.0(1) | 758.3(1) | | 0.2500 | 0.0161[b] | 44 |
| EuAgGe | $KHg_2$ | 467.5(1) | 739.5(2) | 798.1(2) | | 0.2759 | | 42 |
| EuAgGe | $KHg_2$ | 467.0(1) | 740.0(1) | 798.1(1) | | 0.2758 | 0.0371 | 59 |
| EuCdGe | TiNiSi | 770.8(1) | 459.4(1) | 835.2(1) | | 0.2957 | | 38 |
| EuPtGe | LaIrSi | 655.1(1) | = *a* | = *a* | | 0.2811 | 0.0377[b] | 44, 60 |
| EuPtGe | LaIrSi | 654.63(9) | = *a* | = *a* | | 0.2805 | 0.0427 | 12 |
| EuAuGe | EuAuGe | 460.1(1) | 737.1(1) | 788.1(2) | | 0.2673 | 0.0762 | 62 |

[a] These values are equal to those given for the *a* constant. [b] These *R* values result from Rietveld refinements (Bragg residuals).

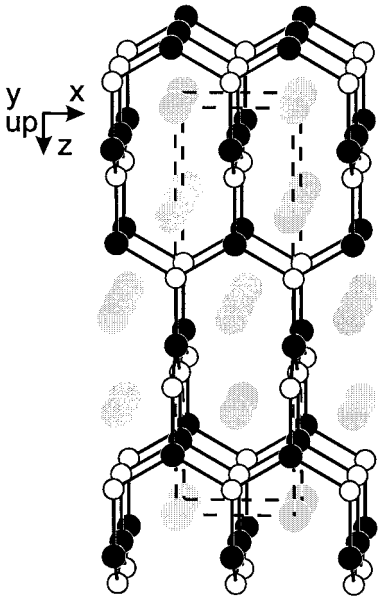


**Figure 8.** Crystal structure of tetragonal EuAlGe, assuming an ordering between aluminum and germanium. The three-dimensional [AlGe] polyanion is outlined.

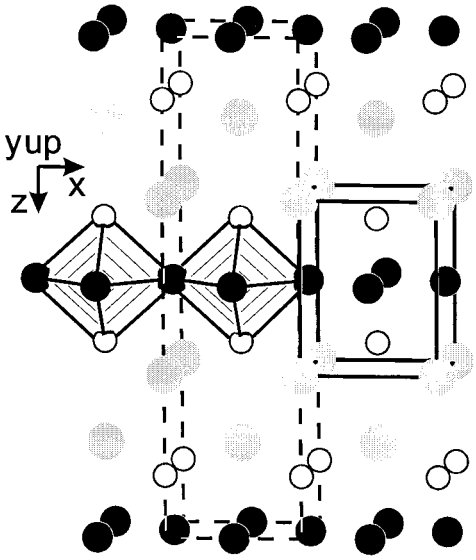


**Figure 9.** Crystal structure of tetragonal EuScGe. A distorted *fcc* ($CeMg_2Si_2$-like) fragment and some compressed $Sc_{4/2}Ge_2$ octahedra are outlined.

the formula $Eu^{2+}Zn^{2+}Ge^{4-}$ with eight valence electrons in the planar network. This is also the case for graphite and for the fully intercalated heterographite LiBC[71] which is isotypic with EuZnGe.

Like EuPdSi and EuPtSi (see preceding chapter), EuPtGe adopts the LaIrSi type structure (space group $P2_13$, Figure 6). The X-ray powder investigation[60] was fully confirmed by single-crystal data.[12] Within the three-dimensional [PtGe] polyanion each platinum atom has three germanium neighbors and vice versa. The Pt−Ge distances of 238 are remarkably shorter than the sum of the metallic single bond radii[33] of 252 pm for platinum and germanium, indicating strong covalent bonding within the polyanion.

EuAgGe[42,59] crystallizes with the $KHg_2$ type structure (space group *Imma*, Figure 2) with a statistical distribution of the silver and germanium atoms on the mercury position of $KHg_2$. A refinement of the occupancy parameters[59] leads to the composition $EuAg_{0.98(2)}Ge_{1.02(2)}$. No significant deviations from the ideal composition was observed. Film data of several single crystals gave no indication for long-range ordering between the silver and germanium atoms.[59]

EuAuGe[62] crystallizes with its own structure type (space group *Imm*2). Only NaAuGe[72] and CaPdGe[44] are isotypic with this europium compound. The EuAuGe structure represents an ordering variant of the $KHg_2$ type. A perspective view of the EuAuGe structure is presented in Figure 12. The structure consists of undulated, distorted $Au_3Ge_3$ hexagonal networks which are connected via weak homonuclear Au−Au (316 pm) and Ge−Ge (277 pm) interlayer interactions. The europium atoms fill the large voids between these networks. The Au−Au and Ge−Ge distances, however, are somewhat longer than in the elements: 288 pm in fcc gold and 245 pm in germanium.[65] In the TiNiSi type ordering variant (Figure 1), there occur only heteronuclear interlayer interactions.

**3.6. Equiatomic Stannides EuTSn.** The nine stannides listed in Table 5 crystallize in four different structure types. EuCuSn[73] and EuAgSn[42,73,74] adopt the $KHg_2$ type structure (space group *Imma*) with a statistical distribution of the transition metal and tin atoms on the mercury site of $KHg_2$. The structures of both stannides have been refined from single-crystal X-ray

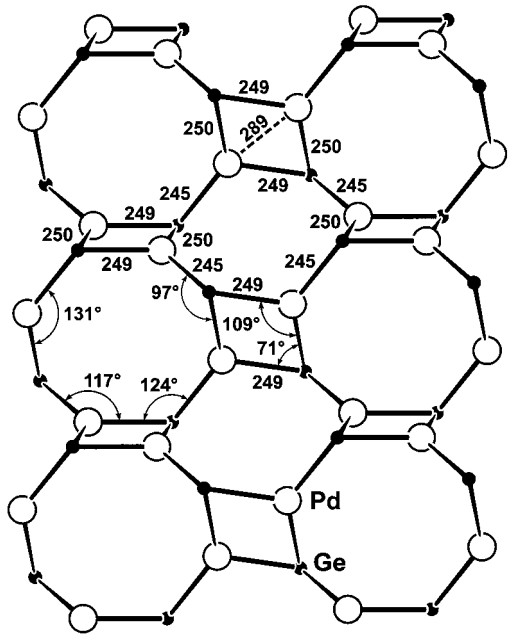


**Figure 10.** Cutout of the two-dimensionally infinite [PdGe] polyanion in EuPdGe. Some relevant bond lengths and bond angles within the $4.8^2$ nets are given.

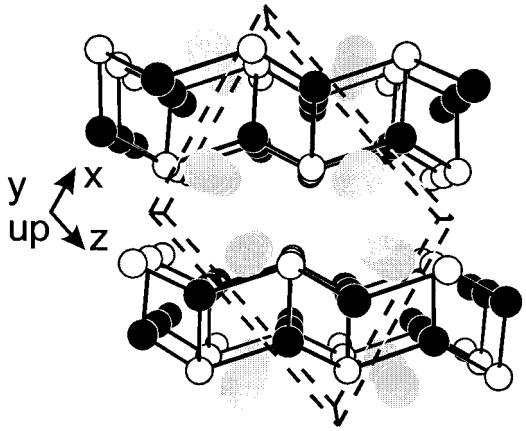


**Figure 11.** Perspective view of the EuPdGe structure along the monoclinic axis. The strongly folded [PdGe] polyanions are outlined.

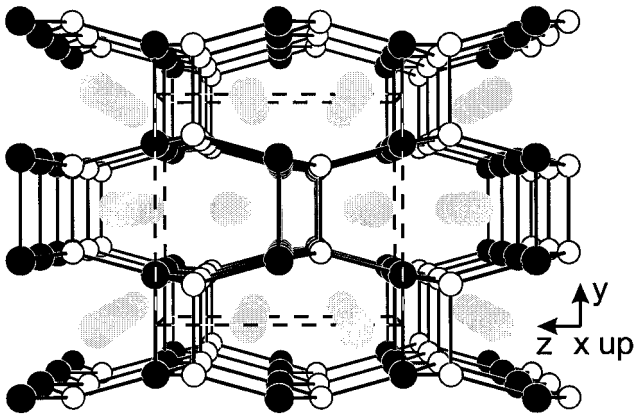


**Figure 12.** Perspective view of the EuAuGe structure along the *x* axis. The three-dimensional [AuGe] polyanion is outlined.

data.[73] These and the X-ray powder investigations gave no indication (superstructure reflections) for long-range ordering of the transition metal and tin atoms. Refinements of the occupancy parameters lead to the formulae $EuCu_{0.96(2)}Sn_{1.04(2)}$ and $EuAg_{1.01(4)}Sn_{0.99(4)}$. No significant deviation from the ideal compositions were observed. The [CuSn] and [AgSn] polyanions (Figure 2) have a pronounced two-dimensional character. The average Cu−Sn and Ag−Sn distances of 273 and 283 pm within the puckered hexagonal networks are significantly smaller than the interlayer distances of 307 and 315 pm.

EuMgSn,[39] EuZnSn,[35,38] EuPdSn,[44,75,76] and EuPtSn[44,76] crystallize with the TiNiSi type structure (space group *Pnma*, Figure 1). While EuMgSn has only been characterized on the basis of X-ray powder data, single-crystal data are available for the other stannides. In a previous study based on X-ray powder data, EuZnSn[38] was found to be isotypic with $KHg_2$; however, a subsequent single-crystal study[35] revealed weak superstructure reflections, indicating an ordering between zinc and tin. The structure of EuZnSn contains a pronounced two-dimensional [ZnSn] polyanion with shorter intralayer (278 pm) and longer interlayer (305 pm) Zn−Sn distances. To a first approximation, EuZnSn may be described as a Zintl phase according to the formula $Eu^{2+}Zn^{2+}Sn^{4-}$, with eight valence electrons within the two-dimensional [ZnSn] polyanions. In contrast to EuZnGe, the [ZnSn] polyanion in EuZnSn is orthorhombically distorted and slightly puckered.

Although these four stannides crystallize with the TiNiSi type in space group *Pnma*, the ordering between the transition metal and tin atoms is different in EuZnSn with respect to EuPdSn and EuPtSn. Because of the puckering and the orthorhombic distortions of the polyanions, rhombic $T_2Sn_2$ units emerge between the distorted hexagonal sheets (Figure 13). In these rhombic $T_2Sn_2$ units, the more electronegative atoms (i.e., Pd and Pt in EuPdSn and EuPtSn and Sn in EuZnSn) occupy the energetically favored position with the maximum distance. Thus, the transition metal and tin positions in EuPdSn and EuZnSn are exchanged with respect to each other. These ordering variants have theoretically been investigated by extended Hückel calculations for several analogous calcium compounds.[78] The ordering in EuMgSn is most likely as in EuZnSn since the tin atoms are by far the most electronegative component of this compound.

EuAuSn[77] crystallizes with a pronounced $KHg_2$ type subcell; however, weak additional reflections require a quintupled *b* axis. The complex superstructure (space group *Imm*2) was determined from single-crystal data. The EuAuSn structure contains several structural fragments of the TiNiSi type; however, there occur six crystallographically different europium sites. The coordination polyhedra of these europium atoms are shown in Figure 14. The Au−Sn intralayer distances within the different $Au_3Sn_3$ hexagons vary from 276 to 283 pm with an average value of 278 pm. This average Au−Sn distance is only slightly larger than the sum of the metallic single bond radii of 274 pm for gold and tin,[33] indicating essentially covalent bonding within these hexagons. Between the hexagons there occur heteronuclear Au−Sn (304 and 310 pm) as well as homonuclear Au−Au (334 and 335 pm) and Sn−Sn (300 pm) contacts connecting the distorted hexagonal sheets to a three-dimensionally infinite [AuSn] polyanion.

**Table 5. Lattice Constants and Residuals for the Stannides EuTSn (T = Mg, Cu, Zn, Pd, Ag, Cd, Pt, Au, Hg)**

| compd | type | *a* (pm) | *b* (pm) | *c* (pm) | *V* (nm$^3$) | *R* value | ref |
|---|---|---|---|---|---|---|---|
| EuMgSn | TiNiSi | 807.5(3) | 485.1(2) | 874.9(2) | 0.3427 | | 39 |
| EuCuSn | $KHg_2$ | 470.0(1) | 771.3(2) | 802.1(2) | 0.2908 | 0.0624 | 73 |
| EuZnSn | $KHg_2$ | 477.0(1) | 787.2(4) | 808.5(3) | 0.3036 | | 38 |
| EuZnSn | TiNiSi | 789.4(1) | 476.7(1) | 807.9(1) | 0.3040 | 0.0955 | 35 |
| EuPdSn | TiNiSi | 750.3(1) | 468.8(1) | 805.0(1) | 0.2832 | 0.0291[b] | 44 |
| EuPdSn | TiNiSi | 749.8 | 468.2 | 803.9 | 0.2822 | | 75 |
| EuPdSn | TiNiSi | 751.24(9) | 469.15(6) | 804.31(9) | 0.2835 | 0.0617 | 76 |
| EuAgSn | $KHg_2$ | 488.6(2) | 761.9(5) | 838.4(4) | 0.3121 | | 42 |
| EuAgSn | $KHg_2$ | 487.8 | 763.0 | 839.6 | 0.3125 | | 74 |
| EuAgSn | $KHg_2$ | 488.1(1) | 768.4(1) | 837.3(2) | 0.3140 | 0.0444 | 73 |
| EuCdSn | LiGaGe | 492.7(1) | = *a*[a] | 790.7(2) | 0.1662 | | 38 |
| EuPtSn | TiNiSi | 751.3(1) | 466.2(1) | 790.9(1) | 0.2770 | 0.0285[b] | 44 |
| EuPtSn | TiNiSi | 753.38(7) | 467.72(4) | 793.08(7) | 0.2795 | 0.0711 | 76 |
| EuAuSn | EuAuSn | 479.1(1) | 3833.6(5) | 820.1(1) | 1.5063 | 0.0834 | 77 |
| EuHgSn | LiGaGe | 488.5(1) | = *a* | 792.7(3) | 0.1638 | | 39 |

[a] These values are equal to those given for the *a* constant. [b] These *R* values result from Rietveld refinements (Bragg residuals).

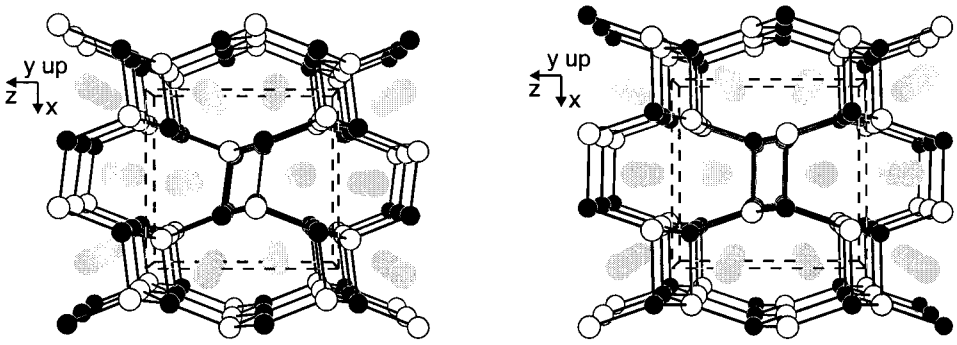


**Figure 13.** Perspective view of the EuPdSn and EuZnSn structure along the *y* axis. The three-dimensional [PdSn] and [ZnSn] polyanions are outlined.

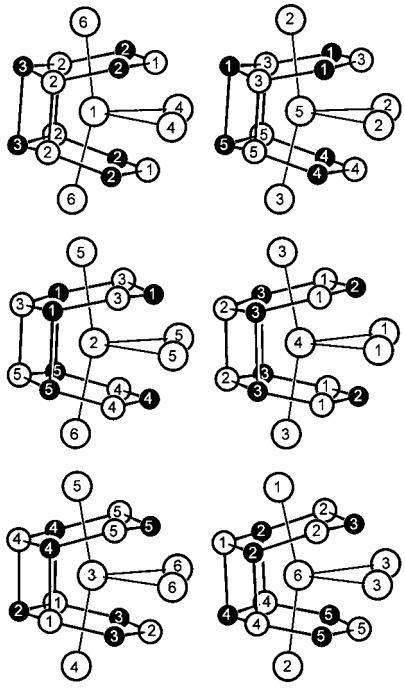

**Figure 14.** Near-neighbor environments of the six crystallographically different europium positions in EuAuSn.

EuCdSn[38] and EuHgSn[39] were characterized on the basis of X-ray powder patterns. According to these data both stannides adopt the LiGaGe type structure (Figure 15), a ternary ordered derivative of the Zintl phase $CaIn_2$.[79] The ordering between cadmium (mercury) and tin can only be determined from the change of the subcell intensities. Space group $P6_3mc$ (LiGaGe type)

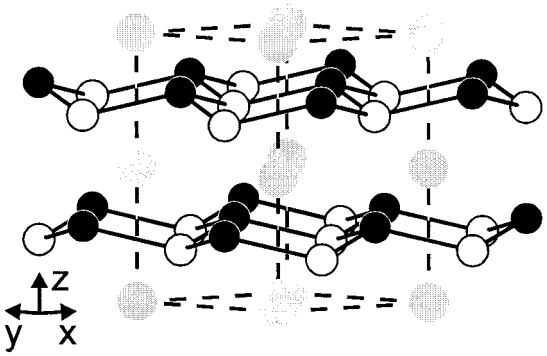


**Figure 15.** Crystal structure of hexagonal EuCdSn. The unit cell is drawn with the lattice constants of EuCdSn and the atomic parameters of DyCuSn.[81]

is a "translationengleiche" subgroup of index 2 (t2) of space group $P6_3/mmc$ ($CaIn_2$ type). Precise single-crystal data are thus desirable to determine the ordering within the polyanions and the free *z* parameters of all positions since the degree of puckering of the hexagons fully results from these *z* parameters. Depending on the puckering, such structures show two- or three-dimensional polyanions.[80] To a first approximation EuCdSn and EuHgSn can be described as Zintl phases according to the formulae $Eu^{2+}Cd^{2+}Sn^{4-}$ and $Eu^{2+}Hg^{2+}Sn^{4-}$.

**3.7. Equiatomic Plumbides EuTPb.** Most plumbides (Table 6) are characterized only from X-ray powder data. The preparation of such samples is often very difficult. In contrast to the mainly moisture stable silicides, germanides and stannides, the plumbides already deteriorate in the presence of moist air. Furthermore, the growth of even small single crystals is not easy.

**Table 6. Lattice Constants and Residuals for the Plumbides EuTPb (T = Mg, Zn, Pd, Ag, Cd, Au, Hg)**

| compd | type | *a* (pm) | *b* (pm) | *c* (pm) | *V* (nm$^3$) | *R* value | ref |
|---|---|---|---|---|---|---|---|
| EuMgPb | TiNiSi | 811.7(2) | 486.75(1) | 889.0(2) | 0.3512 | | 39 |
| EuZnPb | $KHg_2$ | 482.7(1) | 796.8(2) | 823.7(2) | 0.3168 | | 38 |
| EuPdPb | TiNiSi | 751.9(1) | 475.8(1) | 827.1(1) | 0.2959 | 0.0135[b] | 44 |
| EuAgPb | $KHg_2$ | 495.1(2) | 766.8(4) | 855.6(4) | 0.3248 | | 42 |
| EuCdPb | LiGaGe | 492.9(1) | = *a*[a] | 790.0(3) | 0.1662 | | 38 |
| EuAuPb | $KHg_2$ | 487.0(1) | 763.3(3) | 841.2(3) | 0.3127 | 0.0427 | 82 |
| EuHgPb | LiGaGe | 499.6(3) | = *a* | 778.7(6) | 0.1683 | | 39 |

[a] These values are equal to those given for the *a* constant. [b] This *R* value results from Rietveld refinement (Bragg residual).

**Table 7. Lattice Constants, Structure Types, and Residuals for the Phospides EuTP (T = Cu, Ag, Au, Ni, Pd, Pt, Ir, Li)**

| compd | type | *a* (pm) | *b* (pm) | *c* (pm) | *V* (nm$^3$) | *R* value | ref(s) |
|---|---|---|---|---|---|---|---|
| EuCuP | ZrBeSi | 412.3 | = *a*[a] | 820.0 | 0.1207 | | 13 |
| EuAgP | ZrBeSi | 439.5 | = *a* | 805.7 | 0.1348 | | 13 |
| EuAuP | ZrBeSi | 431.3 | = *a* | 825.8 | 0.1330 | | 13 |
| $\beta$-EuNiP | $\beta$-EuPtP | 395.2(1) | = *a* | 829.6(1) | 0.1122 | 0.036 | 83 |
| $\gamma$-EuNiP | $\gamma$-EuPtP | 394.4(1) | = *a* | 816.1(1) | 0.1099 | 0.044 | 83 |
| $\beta$-EuPdP | $\beta$-EuPtP | 414.6(1) | = *a* | 829.3(3) | 0.1235 | 0.016 | 84 |
| $\gamma$-EuPdP | $\gamma$-EuPtP | 415.0(1) | = *a* | 811.2(1) | 0.1210 | 0.019 | 84 |
| $\alpha$-EuPtP | ZrBeSi | 408.6(1) | = *a* | 863.0(2) | 0.1248 | 0.036 | 85 |
| $\beta$-EuPtP | $\beta$-EuPtP | 409.0(1) | = *a* | 838.4(2) | 0.1215 | 0.017 | 85 |
| $\gamma$-EuPtP | $\gamma$-EuPtP | 410.3(1) | = *a* | 825.6(2) | 0.1204 | 0.021 | 85 |
| EuIrP | LaIrSi | 627.2(1) | = *a* | = *a* | 0.2467 | | 86 |
| EuLiP | TiNiSi | 737.0(1) | 436.3(1) | 782.6(2) | 0.2516 | | 87, 88 |

[a] These values are equal to those given for the *a* constant.

EuZnPb,[38] EuAgPb,[42] and EuAuPb[82] crystallize with the $KHg_2$ type structure (space group *Imma*, Figure 2) with a statistical distribution of the transition metal and lead atoms on the mercury site. While the zinc and silver plumbides have been characterized only through X-ray powder data, the structure of the gold compound was refined from single-crystal data. The different X-ray investigations gave no indication for long-range ordering. In contrast, superstructure reflections were observed on the powder patterns of EuMgPb[39] and EuPdPb,[44] indicating an ordering of the TiNiSi type (space group *Pnma*, Figure 1).

In analogy to the respective stannides, also EuCdPb[38] and EuHgPb[39] adopt the structure of LiGaGe (space group $P6_3mc$, Figure 15) and may be written as $Eu^{2+}Cd^{2+}Pb^{4-}$ and $Eu^{2+}Hg^{2+}Pb^{4-}$. For these two plumbides single-crystal data would help to determine the ordering and puckering of the polyanions.

**3.8. Equiatomic Phosphides EuTP.** Equiatomic phosphides of the coin metals were first investigated by Schuster and co-workers in 1981.[13] On the basis of X-ray powder data, the hexagonal ZrBeSi structure (space group $P6_3/mmc$) was assigned. Planar hexagons of ordered transition metal (T) and P atoms form the two-dimensional $[TP]^{2-}$ polyanion. The *c* lattice parameter is doubled compared with the simple $AlB_2$ type, since every other layer of $T_3P_3$ hexagons is rotated by 60° (Table 7). A small degree of puckering of the planar layers toward the LiGaGe type structure (Figure 15) cannot be ruled out, since single-crystal data are not available. A puckering results only in small changes of the subcell intensities. These minor differences can only reliably be determined from precise single-crystal data. The formulae of these coin metal phosphides may to a first approximation be written as $Eu^{2+}T^{1+}P^{3-}$ in agreement with the Zintl concept. The divalent oxidation state of the europium atoms is confirmed by magnetic measurements.[13] Due to the electron precise formulation the compounds with T = Cu, Ag, Au, and Li might be semiconductors; however, investigations of the transport properties have not yet been reported.

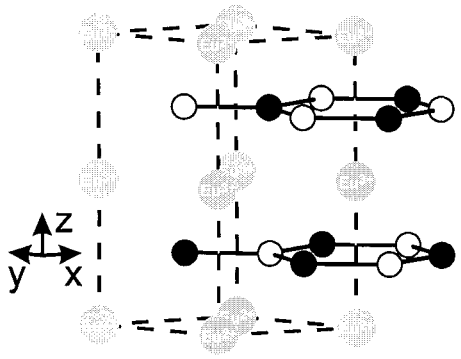


**Figure 16.** Crystal structure of trigonal $\gamma$-EuPtP. The [PtP]-planes are shifted from $z = 1/4$ and $z = 3/4$ (ZrBeSi type) toward the $Eu^{3+}$ atoms.

In contrast to the coin metal compounds with divalent europium, different europium valence states for the equiatomic phosphides with T = Ni, Pd and Pt were observed. These valence instabilities were first discovered for EuPtP.[89] The structures of EuNiP, EuPdP, and EuPtP are closely related to the ZrBeSi type, but deviations occur with dependence of the europium valence state. This behavior is temperature dependent and tends toward trivalent europium ingoing to lower temperatures.[89,90] Normally, intermediate valence states are caused by a fast fluctuation (frequencies of about $10^{15}$ Hz) between the $4f^7$ ($Eu^{2+}$) and $4f^6$ ($Eu^{3+}$) configuration. An intriguing feature is the occurrence of a quasi-static coexistence of $Eu^{2+}$ and $Eu^{3+}$, as confirmed by Mössbauer experiments and single-crystal structure determinations.[91] It is worthwhile to note that this static mixed valence in a metallic system is unique in solid-state chemistry. When the $Eu^{2+}/Eu^{3+}$ ratio is close to 1:1, i.e., the mean valence $\nu = 2.5$, an ordering of the europium atoms of different valence state takes place. Along the *c* axis alternating planes of (almost pure) $Eu^{2+}$ and $Eu^{3+}$ are formed. As a consequence, the $[TP]^{\nu-}$ polyanions move toward the $Eu^{3+}$ atoms due to their

**Table 8. Lattice Constants, Structure Types, and Residuals for the Arsenides EuTAs (T = Cu, Ag, Au, Pd, Pt, Li)**

| compd | type | *a* (pm) | *b* (pm) | *c* (pm) | *V* (nm$^3$) | *R* value | ref(s) |
|---|---|---|---|---|---|---|---|
| EuCuAs | ZrBeSi | 425.4 | = *a*[a] | 827.4 | 0.1297 | | 93 |
| EuAgAs | ZrBeSi | 451.6 | = *a* | 810.7 | 0.1432 | 0.06 | 13 |
| EuAuAs | ZrBeSi | 444.5 | = *a* | 828.5 | 0.1418 | | 13 |
| α-EuPdAs | ZrBeSi | 426.4(1) | = *a* | 853.1(3) | 0.1343 | 0.033 | 14 |
| *β*-EuPdAs | *β*-EuPtP | 425.9(1) | = *a* | 834.3(3) | 0.1311 | 0.037 | 14 |
| EuPtAs | LaPtSi | 423.0 | = *a* | 1487.8 | 0.2662 | 0.042 | 94 |
| EuLiAs | TiNiSi | 754.3(1) | 448.5(1) | 797.8(2) | 0.2699 | | 87, 88 |

[a] These values are equal to those given for the *a* constant.

**Table 9. Lattice Constants, Structure Types, and Residuals for the Antimonides EuTSb (T = Cu, Ag, Au, Pd, Pt, Li)**

| compd | type | *a* (pm) | *b* (pm) | *c* (pm) | *V* (nm$^3$) | *R* value | ref(s) |
|---|---|---|---|---|---|---|---|
| EuCuSb | ZrBeSi | 451.2 | = *a*[a] | 854.2 | 0.1506 | | 13 |
| EuAgSb | ZrBeSi | 475.5 | = *a* | 828.3 | 0.1622 | | 13 |
| EuAuSb | ZrBeSi | 466.9 | = *a* | 848.6 | 0.1602 | | 13 |
| EuPdSb | TiNiSi | 762.7 | 469.5 | 792.5 | 0.2838 | | 95 |
| EuPtSb | TiNiSi | 758.1(2) | 464.2(1) | 789.3(2) | 0.2778 | 0.028 | 94 |
| EuLiSb | TiNiSi | 791.4(3) | 477.6(1) | 835.8(2) | 0.3159 | | 87, 88 |

[a] These values are equal to those given for the *a* constant.

smaller radius. The space group symmetry is reduced from hexagonal ($P6_3/mmc$, ZrBeSi type) to trigonal ($P\bar{3}m1$). This is the structure of γ-EuPtP below 180 K (Figure 16).

When the temperature rises, the mean europium valence changes within two first-order phase transitions abruptly to $\nu \approx 2.35$ at 180 K and to $\nu \approx 2.10$ at 235 K.[85,89] The structure that is stable between 180 and 235 K is called the *β*-EuPtP type. Here, microdomains of $Eu^{2+}$ and $Eu^{3+}$, each smaller than the X-ray coherence length, are formed. For this structure type, hexagonal symmetry is emulated by the collective arrangement even if each microdomain is best descibed with the trigonal space group $P\bar{3}m1$.[85,89] In all cases the $[PtP]^{\nu-}$ polyanions remain nearly planar. Above 235 K almost all europium atoms are in the divalent oxidation state and consequently α-EuPtP adopts the ZrBeSi type at room temperature. The analogous EuTP compounds with T = Ni and Pd essentially show the same behavior as EuPtP. Differences are mainly due to the transition temperatures. EuNiP forms no α-form with ZrBeSi structure. Details about the physical properties are reviewed in chapter 5.

A phase transition toward the γ-form is also induced by applying a static pressure of 2.6 GPa on EuPdP.[92] Structural details are not known, because no high pressure single-crystal data of EuPdP are available. Only two equiatomic EuTP phosphides with other T components than coin metal or Ni-triade elements are known. EuIrP[86] crystallizes with the cubic LaIrSi type, as described in detail for EuPdSi and EuPtSi in chapter 3.5 (Figure 6). Each iridium atom in EuIrP has three phosphorus neighbors in a nearly trigonal-planar coordination.

EuLiP[87,88] adopts the TiNiSi type (see Figure 1). Within the three-dimensional puckered network of $Li_3P_3$ hexagons each lithium atom has a distorted tetrahedral environment of phosphorus atoms. The formula of EuLiP can, to a first approximation, be written as $Eu^{2+}Li^{+}P^{3-}$. The divalent oxidation state of the europium atoms was confirmed by susceptibility measurements (see chapter 5).

**3.9. Equiatomic Arsenides EuTAs.** Seven arsenides EuTAs are reported in the literature. Their lattice constants and structure types are listed in Table 8. Again the coin metal representatives form the ZrBeSi type with divalent europium.[13,93] The $[AgAs]^{2-}$ polyanions in EuAgAs are not puckered as is evident from single-crystal X-ray data[13] and this is most likely the case for the Cu and Au compounds.

In α-EuPdAs a certain amount of trivalent europium atoms occurs resulting in a mean valence of $\nu = 2.14$. The structure is related to the ZrBeSi type, although a slight puckering of the $[PdAs]^{\nu-}$ layers was observed.[14] On cooling, the europium valence jumps to $\nu = 2.35$ and the *c* lattice parameter decreases abruptly form 855 to 835 pm within the phase transition at 180 K.[14] Below this temperature *β*-EuPdAs adopts the *β*-EuPtP microdomain structure as described in the previous chapter. *β*-EuPdAs does not transform to the trigonal γ-EuPtP structure at lower temperatures, i.e., the mean Eu valence of $\nu = 2.5$ is not reached.

Surprisingly EuPtAs[94] does not crystallize with the hexagonal ZrBeSi type structure. It is the only known europium pnictide which adopts the tetragonal body-centered LaPtSi type (space group $I4_1md$), a ternary ordered variant of the α-$ThSi_2$ structure (see chapter 3.6, Figure 7). The ordering of Pt and P on the Si site is confirmed by single-crystal X-ray data. In contrast to the $AlB_2$ derivatives with two-dimensional networks, the phosphorus and platinum atoms form a three-dimensional $[PtP]^{2-}$ polyanion with Pt in nearly trigonal planar coordination.

EuLiAs crystallizes with the orthorhombic TiNiSi structure (Figure 1) with an ordered arrangement of lithium and arsenic atoms. According to Zintl's concept, the compound may be written as $Eu^{2+}Li^{1+}As^{3-}$, assuming divalent europium and a full charge transfer to the more electronegative arsenic atoms. This precise electron description of EuLiAs and the coin metal compounds suggests semiconducting behavior, however, conductivity data have not yet been reported.

**3.10. Equiatomic Antimonides EuTSb.** Six antimonides with the monovalent metals Cu, Au, Ag, and Li as well as with palladium and platinum have been reported (Table 9). Like for the phosphides and arsenides, the coin metal antimonides crystallize with the ZrBeSi type structure as determined by X-ray powder diffractometry.[13] A small degree of puckering of the $[TSb]^{2-}$ polyanionic layers, as in the LiGaGe-type, may

**Table 10. Lattice Constants, Structure Types, and Residuals for the Bismuthides EuTBi (T = Cu, Ag, Au, Li)**

| compd | type | *a* (pm) | *b* (pm) | *c* (pm) | *V* (nm$^3$) | *R* value | ref(s) |
|---|---|---|---|---|---|---|---|
| EuCuBi | ZrBeSi | 462.2 | = *a*[a] | 853.6 | 0.1579 | | 13 |
| EuAgBi | ZrBeSi | 487.7 | = *a* | 813.9 | 0.1677 | | 13 |
| EuAuBi | LiGaGe | 479.9(1) | = *a* | 829.5(2) | 0.1654 | | 96 |
| EuLiBi | TiNiSi | 798.1(1) | 484.8(1) | 848.3(2) | 0.3282 | | 87, 88 |

[a] These values are equal to those given for the *a* constant.

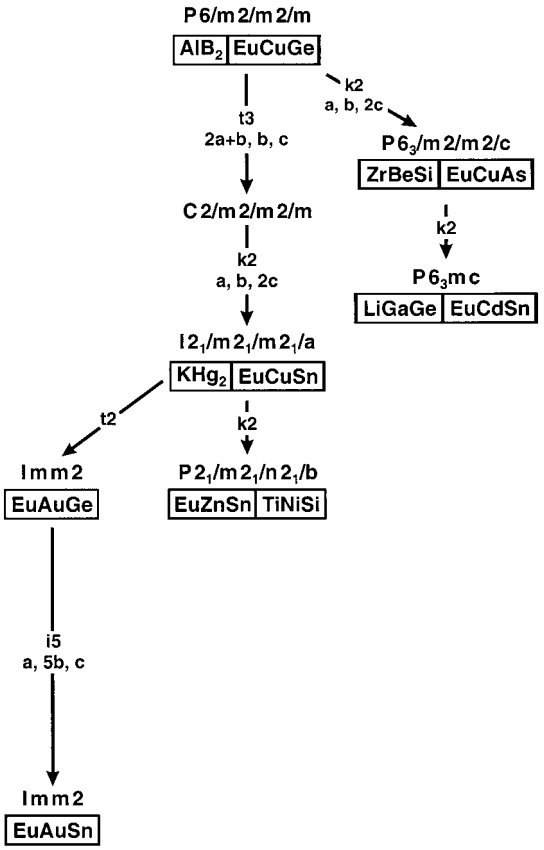


**Figure 17.** Group−subgroup relations in the Bärnighausen formalism[97,98] for some structure types derived from the aristotype $AlB_2$. The indices of the "translationengleiche" (t), "klassengleiche" (k), and isomorphic (i) transitions, as well as the unit cell transformations are presented. For each structure type, an example for an EuTX compound is also given. For the TiNiSi structure the nonstandard setting *Pmnb* is used to avoid a noncyclic cell transformation.

occur for the antimonides. There is a general trend for these compounds to form more puckered hexagons (orthorhombic TiNiSi type) when the quotient of the atomic radii $r_{Eu}/r_{(TSb)}$ becomes smaller.[94] In the case of the EuTSb antimonides with T = coin metals, single-crystal data are therefore highly desirable to determine the stability range of the ZrBeSi type with respect to the radii.

According to these arguments, the TiNiSi structure first occurs for the antimonides EuTSb with T = Pd and Pt. The transition metal atoms are coordinated to four antimony atoms in the form of a strongly distorted tetrahedron. The $T_3Sb_3$ hexagons are strongly puckered and consequently the $[TSb]^{2-}$ polyanion is now three-dimensional, due to bonding interlayer T−Sb contacts. The europium atoms are embedded within these networks.

EuLiSb also adopts the TiNiSi type although one would expect the ZrBeSi type due to the larger $r_{Eu}/r_{(LiSb)}$ ratio and the electrovalent description $Eu^{2+}Li^{+}Sb^{3-}$ like

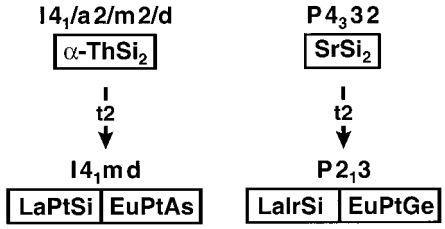


**Figure 18.** Group-subgroup relations for the structures of α-$ThSi_2$ and LaPtSi (left-hand part) as well as $SrSi_2$ and LaIrSi (right-hand drawing). The indices of the "translationengleiche" (t) transitions are presented. For both ternary ordered versions also an example for an EuTX compound is given.

for the coin metal compounds.

**3.11. Equiatomic Bismuthides EuTBi.** The ternary systems with bismuth have not been intensively investigated. Schuster and co-workeres[13] reported on the first equiatomic bismuthides, EuCuBi and EuAgBi, and they assigned the ZrBeSi type for these compounds on the basis of X-ray powder data. Later Merlo and co-workers[96] synthesized EuAuBi with LiGaGe type structure (Table 10). Here the $[AuBi]^{2-}$ polyanionic layers show a slight puckering. Since all structures of the bismuthides were assigned exclusively on the basis of powder diffraction data, single-crystal investigations are desirable to determine the symmetry of the polyanionic layers. EuLiBi crystallizes with the TiNiSi type structure.[87,88]

**3.12. Structural Classification via Group−Subgroup Schemes.** A total of 72 different equiatomic EuTX compounds has been reviewed in chapters 3.1 to 3.11. These compounds crystallize with 12 different structure types. Sixty-two of these 72 intermetallic compounds have planar or puckered $T_3X_3$ hexagons as a common structural motif. These structures are all derived from the well-known aristotype $AlB_2$. A concise and compact way to classify such a large number of related structure types is the introduction of group−subgroup schemes in the formalism of Bärnighausen[97,98] (Figures 17 and 18). In the structures of the aristotype $AlB_2$ (EuCuGe) and the ternary ordered version ZrBeSi (EuCuAs) the $T_3X_3$ hexagons are planar, while they become puckered in the LiGaGe (EuCdSn) structure (see Figures 4, 5, and 15). In the orthorhombically distorted structures of $KHg_2$ (EuCuSn), TiNiSi (EuZnSn), EuAuGe, and EuAuSn, the hexagons are even tilted with respect to each other (see Figures 1, 2, 12, and 14).

The group−subgroup scheme in Figure 17 thus reflects the evaluation of the symmetry reduction for the respective structure types. Because of symmetry restrictions, those ternary EuTX compounds with $AlB_2$ and $KHg_2$ type structure show a statistical occupancy of the transition metal and X atoms on the boron and mercury site, respectively. Further decoupling of these positions via symmetry reductions then allows ordered arrangements of the T and X atoms. These group−subgroup

schemes of the $AlB_2$ family are only briefly reviewed here. A very detailed review of the $AlB_2$ family, including 46 different structure types with more than 1500 $AlB_2$ related compounds is given elsewhere.[99]

In Figure 18, we present the group−subgroup schemes for the aristotypes α-$ThSi_2$ and $SrSi_2$. Upon reducing the space-group symmetry via "translationengleiche" symmetry reductions of index 2 (t2) to space groups $I4_1md$ (LaPtSi and EuPtAs) and $P2_13$ (LaIrSi and EuPtGe), an ordering of the transition metal and X atoms on the silicide networks is possible. Six EuTX compounds crystallize with these two structure types.

Besides these structural families, there remain the structures of EuRhGa (PbFCl type), EuNiGe, EuPdGe (both EuNiGe type), and EuScGe ($La_2Sb$ type) within the series of EuTX compounds which are somewhat unique. EuRhGa is the only known gallide until now which crystallizes with the PbFCl structure. With the EuNiGe type, so far only EuPdGe, CaPdGe,[44] and LaNiGa are known.[67] In EuScGe scandium takes the position of a rare earth element and not of a transition metal. Consequently we observe an ordering of scandium and europium on the two crystallographically independent lanthanum sites of the $La_2Sb$ type.

## 4. Chemical Bonding

In comparison with the huge number of crystal structures and the various physical property measurements (chapter 5), the knowledge about chemical bonding in EuTX compounds is rather scarce. The so far available theoretical work is limited on the pnictides and mainly focused on the intermediate valence state of the europium atoms therein.[100−103] Furthermore, chemical bonding in isotypic and related intermetallic compounds with rare earth or alkaline earth metals as electropositive components has been investigated by the extended Hückel and LMTO methods.[78,104−107]

Starting from atomic distances considerations, chemical bonding in EuTX compounds appears to be characterized by covalent bonding between T and X atoms within the negatively polarized polyanions and rather electrostatic interactions to the positively polarized europium atoms. From the viewpoint of electronic structure, Zintl's concept was often used to interpret chemical bonding in EuTX compounds. Europium is the most electropositive component, and consequently two valence electrons should be transferred to the [TX] polyanion to enable covalent bonding between the T and X atoms. Such a charge transfer is expected in view of the course of Pearson's absolute electronegativities.[108] The transition elements T are either in distorted tetrahedral coordination with four covalent bonds or in trigonal-planar environment with three bonds to the neighboring X atoms. In any case, eight valence electrons per [TX] unit should be favorable according to the $8 - N$ rule. In EuTX compounds, however, transition elements are present and it was demonstrated[106] that d orbitals participate in T−X bonding and therefore the d electrons must be taken into account. Thus, the highest number of valence electrons should be 18 per formula unit and indeed no EuTX compound with a valence electron concentration (VEC) > 18 is known. Lower VECs are frequently observed, especially some gallides and indides exist with VEC = 14 and 15, whereas all representatives with group 4 and group 5 elements have VECs ranging from 16 to 18.

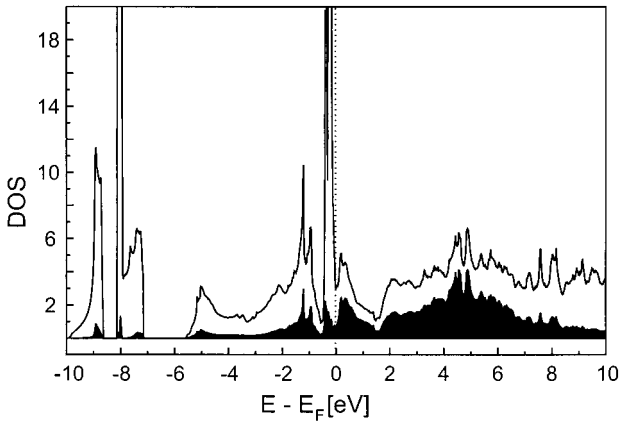


**Figure 19.** Density-of-states (DOS) for EuZnGe and projection of the Eu-5d contribution (shaded area). The Fermi energy is drawn as a dotted line.

The question, to what extend EuTX compounds can be understood as Zintl phases is still under discussion. Electron precise compositions are rather exceptional for EuTX compounds and moreover all electrical conductivity measurements (see chapter 5) yielded metallic behavior. A more detailed picture of the electronic structure and chemical bonding can be derived from band structure calculations. In the following we present the results of first principles LMTO[109] calculations on EuZnGe, EuPdGa, and EuScGe as representative examples for the europium compounds.

For EuZnGe the ionic formula splitting leads to an electron precise formulation $Eu^{2+}Zn^{2+}Ge^{4-}$, as requested from the Zintl concept. The VEC is 18 and consequently the valence band of the $[ZnGe]^{2-}$ polyanion should be completely filled. EuZnGe is thus expected to be a semiconductor, but the experiment shows metallic behavior (see chapter 5, Figure 35).

At first glance, this contradicts Zintl's concept, but it agrees with the density-of-states (DOS) resulting from the band structure calculation. As is evident from Figure 19, no energy gap occurs at the Fermi level. The states at $E_F$ result from an overlap of the Zn−Ge valence band and the conduction band. The latter one is mostly composed of the 5d states of europium (shaded region in Figure 19).

Although the electronic structure calculation shows the typical features of a metal, it also reflects the validity of the Zintl interpretation. To investigate chemical bonding in EuZnGe in more detailed, we have calculated the Zn−Ge crystal orbital Hamilton population (COHP).[110] COHP represents an energy-resolved bonding description based on an energy-partitioning scheme in contrast to the well-known crystal orbital overlap population (COOP),[111] which is an electron-partitioning scheme. Negative values for COHP indicate bonding, positive values antibonding contributions. To make COHP diagrams similar to COOP schemes, we plot −COHP vs energy (Figure 20).

The Fermi level separates bonding and antibonding levels. Zn−Ge bonding states are filled and all antibonding ones are empty. This corresponds exactly to 36 bonding electrons per unit cell, as seen from the COHP vs number of states ($N(\epsilon)$) plot in Figure 21. Zinc and

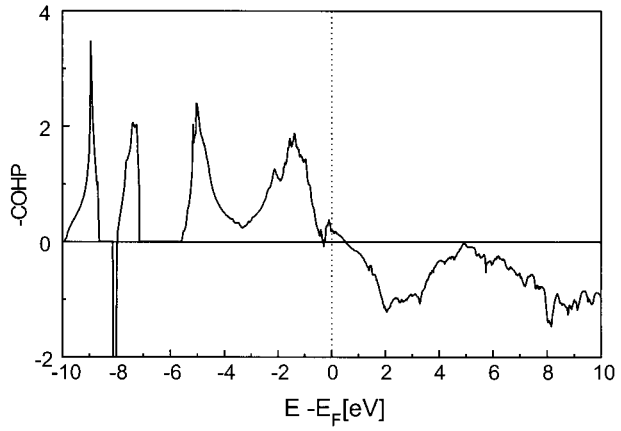


**Figure 20.** COHP vs energy for Zn−Ge bonding in EuZnGe.

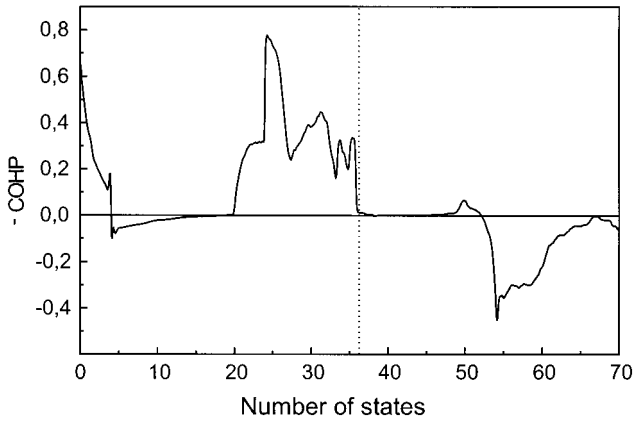


**Figure 21.** Zn−Ge bonding in EuZnGe: COHP vs number of states.

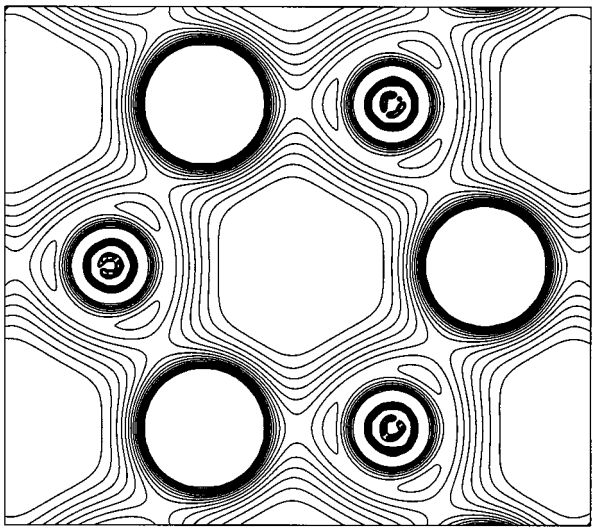

**Figure 22.** Calculated charge density of a $Zn_3Ge_3$ hexagon in EuZnGe; *xy* plane at $z = 1/4$. The contour lines range from 0 to 0.1 $e^-/a_o^3$, where $a_o$ is the Bohr radius.

germanium together can supply only 32 electrons. Consequently, electrons have been transferred from Eu to the Zn−Ge valence band, which is now completely filled with 36 electrons. EuZnGe contains two formula units per unit cell. This corresponds to VEC = 18.

To illustrate chemical bonding in real space, we have calculated the valence electron charge density within the planar hexagons of EuZnGe, shown in Figure 22. Strong covalent bonding between Zn and Ge is clearly visible, the charge density has the highest values along the Zn−Ge bond axis. The maximum bonding electron density is shifted toward the germanium atoms due to their higher electronegativity.[108] With regard to these results of the electronic structure calculations, we can draw the conclusion, that chemical bonding in EuZnGe corresponds to the central idea of Zintl's concept, namely the formation of covalent bonds (Zn−Ge) by using electrons from the electropositive component (Eu). EuZnGe may be classified as a metallic Zintl phase.

Chemical bonding in the hexagonal structures with puckered $T_3X_3$ hexagons was also investigated (see refs 80, 104, 105, and 112 and references therein). Very similar bonding characteristics were observed for the strongly covalent intralayer T−X bonding. As already mentioned in chapter 3.6, the degree of puckering strongly influences the interlayer bonding. Burdett and Miller performed total energy calculations for a hypothetical Si structure with constant volume and investigated the dependence of the puckering angle from the *c*/*a* ratio.[105] These calculations showed the following tendency: the smaller the *c*/*a* ratio of the cells, the greater is the tendency to pucker the $T_3X_3$ hexagons. This was investigated experimentally for the series of LnAuGe germanides.[80,112] With decreasing size of the rare earth element the puckering of the $Au_3Ge_3$ hexagons increases and the *c*/*a* ratio decreases. Consequently the interlayer Au−Ge distances decrease from 386 pm (LaAuGe) via 293 pm (LuAuGe) to 275 pm (ScAuGe), resulting in increasing interlayer Au−Ge bonding. Thus, we observe a continuous transition from two- to three-dimensional [AuGe] polyanions in the series of LnAuGe germanides. This was proven by total valence charge density plots[80] which were calculated with the TB-LMTO-ASA method.[109] Although the atoms in LaAuGe and ScAuGe occupy the same Wyckoff sites in space group $P6_3mc$, one should call their relationship isopointal[27,113] rather than isotypic, in view of the significant differences in chemical bonding.

Band structure calculations for EuTX compounds with TiNiSi or related structures with four-coordinated transition metals T lead to results very similar to EuZnGe. When less than 18 valence electrons per formula unit are available, the bonding states of the TX polyanions cannot be completely filled. The compounds have no electron precise composition and are expected to be metallic. But nevertheless the arguments for the applicability of the Zintl concept given above are reasonable.

Chemical bonding in the TiNiSi family of compounds has recently been intensively studied in the Hoffmann group.[78,107] These calculations revealed an increasing stability for the polyanion when the electron count is increased from 16 to 30 valence electrons (per four formula units). For more than 30 valence electrons destabilization occurs due to filling of T−X antibonding states. The distortions of the $T_3X_3$ hexagons in the polyanions were investigated by structure refinements[35,107] and perfectly match the calculations.

As an example for the series of europium compounds, we present the density-of-states (DOS) of EuPdGa in Figure 23. This compound crystallizes in the orthorhombic TiNiSi type structure ($Z = 4$) with 60 valence electrons per unit cell, i.e., VEC = 15. The expected

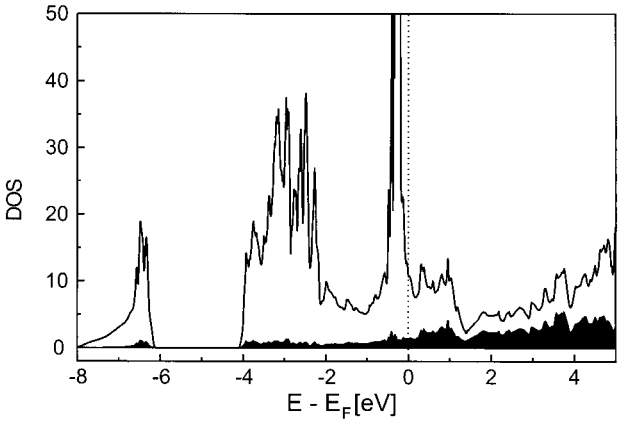


**Figure 23.** Density-of-states (DOS) for EuPdGa with a projection of the Eu-5d orbital contribution (shaded area).

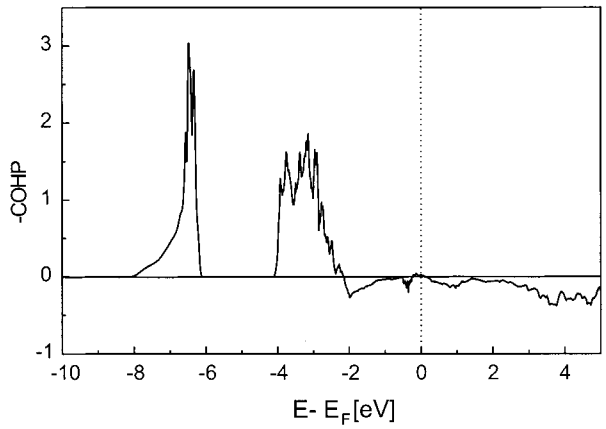


**Figure 24.** COHP diagram for the Pd−Ga bonds in EuPdGa.

metallic behavior is confirmed by the DOS, i.e., no gap occurs at the Fermi level. Like for EuZnGe, the europium states are only partially filled and represent the main contribution to the conduction band at $E_F$.

A remarkable difference appears for the Pd−Ga COHP (Figure 24) compared with the Zn−Ge COHP (Figure 20). In contrast to EuZnGe, the electronic states around the Fermi level are antibonding with respect to the Pd−Ga contacts. The reason for this difference is not the different crystal structures, since a similar effect was also reported for LaPdAs and SrPdAs,[106] both adopting the ZrBeSi structure. A detailed analysis of the electronic structure revealed, that these antibonding states originate from a contribution of the transition metal d orbitals to the T−X bonds. They form bonding and antibonding combinations with the orbitals of the neighboring X atoms.

The requirement for this behavior is an open d shell, i.e., the electron configuration of the transition metal has to be $d^9$ (leading to the formal descriptions $Eu^{2+}Pd^{+}Ga^{3-}$ and $Eu^{2+}Ni^{+}P^{3-}$)[102] or lower. Closed d shells as in $Cu^+$, $Ag^+$, $Au^+$, or $Zn^{2+}$ are contracted and very low in energy, i.e., the spatial extent of the orbitals is small and consequently the interactions with the X atoms are weak. Even in this case the top of the transition metal d band is T−X antibonding, as seen from the sharp negative peak in the COHP curve of EuZnGe at −8 eV (Figure 20). EuTX compounds containing transition metals with $d^{10}$ configurations may be regarded as built up of main group atoms. The T−X valence levels are completely filled at VEC = 18.

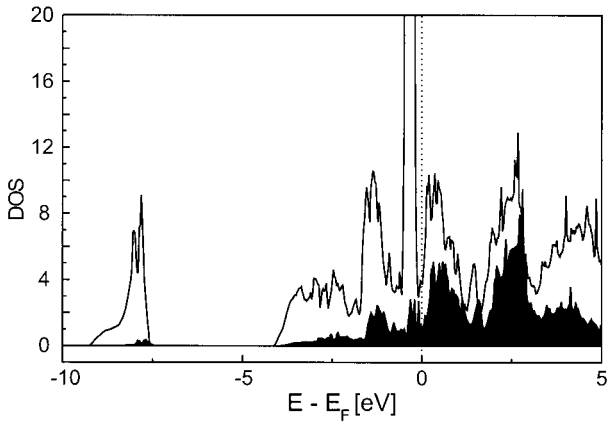


**Figure 25.** Density-of-states (DOS) for EuScGe with a projection of the Sc-3d orbital contribution (shaded area).

However, in the case of open d shell compounds (T = Rh, Ni, Pd, Pt) the T−X bonds are slightly weaker when antibonding states are filled. This was demonstrated for SrPdAs and LaPdAs, both forming the hexagonal ZrBeSi type structure.[106] In SrPdAs the Pd−As distance is shorter (246 pm) than in LaPdAs (253 pm)[14] despite the larger radius of strontium compared with lanthanum. The VECs are 17 in SrPdAs and 18 in LaPdAs. Consequently more antibonding states are filled in LaPdAs and the Pd−As bonds are longer.

Also the family of the orthorhombic $KHg_2$ and TiNiSi related compounds shows transitions from two- to three-dimensional [TX] polyanions, depending on the degree of interlayer T−X bonding. This mechanism is very similar to the one described above for the LnAuGe series and described for the europium compounds on the basis of structure refinements in reference.[35]

As briefly mentioned in chapter 3.5, a special bonding situation is formed in EuScGe. Since no homonuclear Ge−Ge bonds exist in this structure, an ionic formula splitting leads to $Eu^{2+}Sc^{2+}Ge^{4-}$. The divalent character of the europium atoms in EuScGe is evident from $L_{III}$ spectra (see chapter 5). The scandium atoms in EuScGe form planar squares with Sc−Sc distances of 302 pm, significantly shorter than in hcp scandium with an average Sc−Sc distance of 328 pm. It may be assumed that the surplus electron is involved in Sc−Sc bonding. We have proven this assumption by a band structure calculation. Figure 25 shows the calculated DOS with a projection of the Sc-3d orbital contribution. The d levels are indeed partially filled, in agreement with the formal description $Sc^{2+}$. As it is evident from the COHP diagram in Figure 26, these scandium d states are strongly Sc−Sc bonding, reflecting our idea of chemical bonding in EuScGe discussed above.

The Sc−Sc bonding levels are not completely filled. At the same time four identical Sc−Sc contacts occur in the structure of EuScGe. To form four 2-center-2-electron bonds, four electrons per scandium atom would be necessary, but only one is available. The valence electron density of the scandium plane of the EuScGe structure (Figure 27) shows no charge accumulation between the Sc atoms, but a weak maximum in every second square center, indicating multicenter bonding, as it is typical for electron deficient systems.

To locate the bonding electrons, we have calculated the electron localization function ELF[114−116] within the

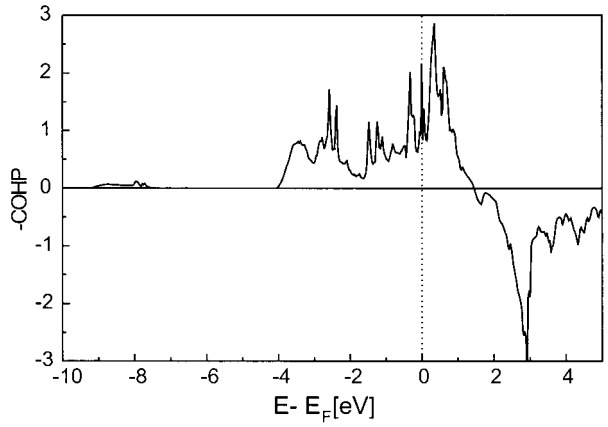


**Figure 26.** Sc−Sc COHP of EuScGe.

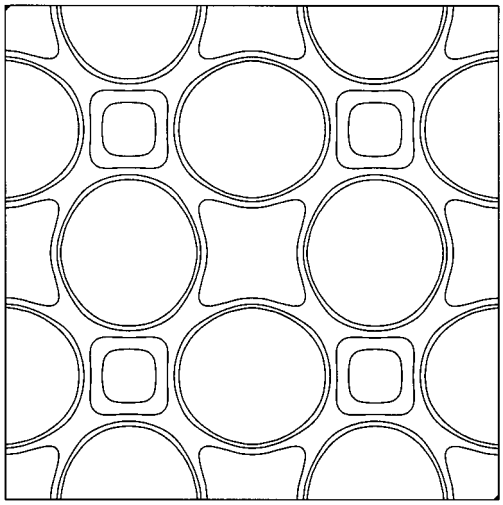

**Figure 27.** Calculated charge density of EuScGe in the *xy* plane at $z = 0$.

plane of scandium atoms. Values of ELF are defined between 0 and 1. Large values (>0.7) mean a high probability of paired electron spins, i.e., regions of either covalent bonds or lone pairs of electrons. The ELF map in Figure 28 renders contour lines from ELF = 0.5 to ELF = 0.9 with an increment of 0.05. The highest values up to 0.9 correspond to the shell structure of the scandium core electrons. Furthermore, ELF maxima (up to 0.78) occur in the center of every second square. This clearly shows the formation of 4-center-2-electron bonds within the scandium planes of EuScGe. Since each scandium atom can supply only one electron to Sc−Sc bonding, the number of 4-center-2-electron bonds must be half the number of scandium atoms. Consequently we observe the bonding electrons located only in every other square center.

In summary chemical bonding in most EuTX compounds is consistent with an extended Zintl formulation. Because of a transfer of the europium valence electrons, the transition metal and X atoms can form two- or three-dimensional polyanions with covalent T−X bonds.

## 5. Chemical and Physical Properties

**5.1. Chemical Properties.** Most of the EuTX compounds have the typical appearance of intermetallic phases. Polycrystalline samples are mostly light gray, while ground powders are dark gray. Single crystals are

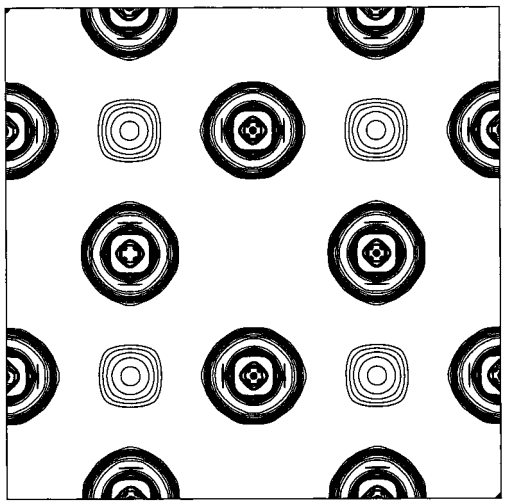

**Figure 28.** Electron localization function of EuScGe in the *xy* plane at $z = 0$.

silvery with metallic luster. Some compounds show colors. EuPtP appears as brass-yellow powder and the coin metal pnictides are grayish blue in powdered form.

The stability of the EuTX compounds in moist air varies significantly. If X is an element of the third or fourth main group, only EuZnIn[35] and the plumbides[82] are moisture sensitive. They completely deteriorate in moist air within a few days. Most aluminides, gallides, indides, silicides, germanides, and stannides are stable in moist air over weeks. The mercury-containing phases EuHgSn and EuHgPb, however, show a rapid deterioration in moist air.[39]

The pnictides show a remarkable chemical stability. To give an example: larger crystals of EuPtP have been prepared in a lead flux. This flux was subsequently dissolved with an oxidizing mixture of 30% $H_2O_2$/acetic acid 1:1. EuPtP resists against these extreme conditions. In general, perfectly shaped single crystals of the EuTX compounds show a larger stability than ground powders due to the much larger surface of the powder.

The mecanical stability of the EuTX compounds is not very high. Most samples are very brittle. They can easily be ground to powders in an agate mortar.

**5.2. Physical Properties.** The various physical properties of the EuTX compounds have intensively been investigated in recent years. These investigations mainly focused on the determination of the oxidation state of the europium atoms. For this purpose, the magnetic properties and $^{151}$Eu Mössbauer spectroscopic data have been most intensively studied. Additionally the electrical conductivity, $L_{III}$ and point contact spectra as well as high-pressure experiments and specific heat measurements have been performed. In the following chapters these different techniques are reviewed separately.

*5.2.1. Magnetic properties.* The experimental data of the greately varying magnetic properties are listed in Table 11. Most EuTX compounds contain divalent europium. The experimental magnetic moments are close to the value of 7.94 $\mu_B$/Eu for the free $Eu^{2+}$ ion.[3] In those cases where the experimental moments are slightly above or below 7.94 $\mu_B$/Eu, the samples most likely contained small amouts of impurities. Down to 2 K no magnetic ordering has been observed for EuPdSi,

**Table 11. Magnetic Properties of Ternary EuTX Compounds[a]**

| compd | ordering type | ordering temperature [K] | $\mu_{exp}$ [$\mu_B$] | $\Theta$ [K] | $\mu_{sm(exp)}$ [$\mu_B$] | $B_C$ [T] | ref(s) |
|---|---|---|---|---|---|---|---|
| | | | Aluminides | | | | |
| EuAuAl | AF | $T_N \approx 50$ | 7.6 | +52 | 5.7 at 2 K | | 19 |
| | | | Gallides | | | | |
| EuCuGa | AF | $T_N = 12$ | | | | | 124 |
| EuZnGa | SG | $T_F = 24(2)$ | 7.86(5) | 17(2) | 4.9(1) at 2 K | | 133 |
| EuPdGa | F | $T_C = 38$ | | | 7.0 at 5 K | | 125 |
| EuAgGa | CW | | | | | | 124 |
| EuPtGa | F | $T_C = 36$ | | | 7.0 at 5 K | | 125 |
| EuAuGa | CW | | | | | | 124 |
| EuAuGa | F | $T_C = 16(1)$ | 7.72(5) | 16(1) | 5.9(1) | | 121 |
| | | | Indides | | | | |
| EuZnIn | AF | $T_N = 8.0(5)$ | 7.80(5) | 6(2) | 4.8(1) | | 123 |
| EuRhIn | F | $T_C = 22.0(5)$ | 7.9(1) | 34(1) | 6.7(1) | | 34 |
| EuPdIn | P | | 7.99 | 40 | | | 31 |
| EuPdIn | MM | $T_N = 13.0(5)$ | 7.6(1) | 13(1) | 5.9(1) | 3.1(1) | 32 |
| EuPdIn | MM | $T_N = 13.0$ | | | 7.0 | 3.4 and 5.1 | 122 |
| EuPtIn | MM | $T_N = 16.0(5)$ | 8.0(1) | 20(2) | 7.0(1) | 1.1and 2.6 | 123 |
| EuAuIn | MM | $T_N = 21.0(5)$ | 7.5(1) | 22(1) | 5.9(1) | 0.25(2) | 32 |
| | | | Silicides | | | | |
| EuPdSi | P | <4.2 K | 7.45 | 9 | | | 41 |
| EuPdSi | P | | 7.9 | | | | 40, 44 |
| EuPtSi | P | <4.2 K | 7.50 | 5 | | | 41 |
| | | | Germanides | | | | |
| EuZnGe | MM | $T_N = 12.2(5)$ | 7.8(1) | 11(1) | 5.8(1) | 0.60(5) | 57 |
| EuPdGe | MM | $T_N = 8.5(5)$ | 8.0(1) | 12(1) | 6.4(1) | 1.5(2) | 128 |
| EuAgGe | SG | $T_F = 18(1)$ | 7.70(5) | −2(1) | 3.3(1) | | 120 |
| EuPtGe | P | <2 K | 7.80(5) | 20(1) | | | 12 |
| EuAuGe | F | $T_C = 32.9(2)$ | 7.40(5) | 34(1) | 6.2(1) | | 62, 120 |
| | | | Stannides | | | | |
| EuCuSn | P | | 7.75(5) | −16(1) | 3.85(5) | | 129 |
| EuZnSn | MM | $T_N = 20.5(2)$ | 7.88(5) | 24(1) | 6.80(5) | 0.7(1) | 117 |
| EuAgSn | MM | $T_N = 6.0(5)$ | 7.96(5) | −31(1) | 3.5(5) | 3.85(5) | 129 |
| EuAgSn | AF | $T_N = 6.5$ | 7.97 | | | | 74 |
| EuPdSn | MM | $T_N = 15.5(5)$ | 7.78(5) | 13(1) | 6.40(5) | 2.5(2) | 129 |
| EuPdSn | AF | $T_N = 13$ | 8.27 | 5 | | | 75 |
| EuPtSn | MM | $T_N = 28.5(2)$ | 8.10(5) | 19(1) | 5.80(5) | 0.8(1) | 129 |
| EuAuSn | MM | $T_N = 8.5(5)$ | 7.6(1) | −8(1) | 3.5(1) | 2.0(2) | 77 |
| | | | Plumbides | | | | |
| EuAuPb | AF | $T_N = 7$ | 6.8(1) | −14(1) | | 2.8(1) | 82 |
| | | | Phosphides | | | | |
| EuNiP | F/VF | $T_C = 40$ | | | | | 91 |
| EuCuP | F | $T_C = 37$ | 7.64 | 41 | | | 13, 126 |
| EuPdP | AF/VF | $T_N = 7.5$ | | | | | 91 |
| EuAgP | F | $T_C = 18$ | 7.52 | 20 | | | 13, 126 |
| EuIrP | F | | 7.53 | 18.2 | | | 86 |
| EuPtP | AF/VF | $T_N = 8.6$ | 7.46 | | | | 89, 130 |
| EuAuP | F | $T_C = 17$ | 7.68 | 22 | | | 13, 126 |
| EuLiP | F | $T_C = 21(1)$ | 7.15 | 39(3) | 5.7(1) | | 118 |
| | | | Arsenides | | | | |
| EuCuAs | MM | $T_N = 18$ | 7.67 | 28 | 6.9 | 0.18 | 119 |
| EuPdAs | VF | | 7.04 | 0 | | | 127 |
| EuAgAs | MM | $T_N = 11$ | 7.45 | 19 | 6.5 | 0.25 | 119 |
| EuAuAs | F | $T_C = 8$ | 7.57 | 11 | | | 13, 126 |
| EuLiAs | MM | $T_N = 9(1)$ | 7.42 | 16(3) | 6.6(1) | <0.5 T | 118 |
| | | | Antimonides | | | | |
| EuCuSb | AF | $T_N = 12$ | 7.72 | 7 | | | 119 |
| EuPdSb | AF | $T_N = 13$ | 8.19 | −35 | 0.3(1) | | 95 |
| EuAgSb | AF | $T_N = 8$ | 7.62 | 2 | | | 119 |
| EuAuSb | AF | $T_N = 10$ | 7.60 | 6 | | | 119 |
| EuLiSb | MM | $T_N = 6.7(4)$ | 8.46 | 4(3) | 7.0(1) | 0.7(2) | 118 |
| | | | Bismuthides | | | | |
| EuCuBi | AF | $T_N = 18$ | 7.65 | −13 | | | 119 |
| EuAgBi | AF | $T_N = 10$ | 7.39 | −4 | | | 119 |
| EuAuBi | AF | $T_N = 8$ | | | | | 119 |
| EuLiBi | SF | $T_N = 7.5(4)$ | 8.43 | 0(3) | 4.7(1) | 1.5(3) | 118 |

[a] Abbreviations: P, paramagnetism; AF, antiferromagnetism; F, ferromagnetism; SG, spin glass behavior; MM, metamagnetism; SF, spin-flop behavior; $\mu_{exp}$, experimental magnetic moment; $T_C$, Curie temperature; $T_N$, Néel temperature; $T_F$, spin freezing temperature; $\Theta$, paramagnetic Curie temperature; $B_C$, critical field; CW, Curie−Weiss behavior, no further data available; VF, valence fluctuation.

EuPtSi, EuPtGe, EuCuSn, and EuAuPb. These compounds remain paramagnetic down to very low temperatures.

All other EuTX compounds show either mixed valency or magnetic ordering. The so far highest ordering temperature was observed for the 50 K antiferromagnet EuAuAl.[19] Antiferromagnetic ordering was also detected for several other EuTX compounds, however, most of them show metamagnetic or spin−flop transitions (antiparallel to parallel spin alignments) at different critical

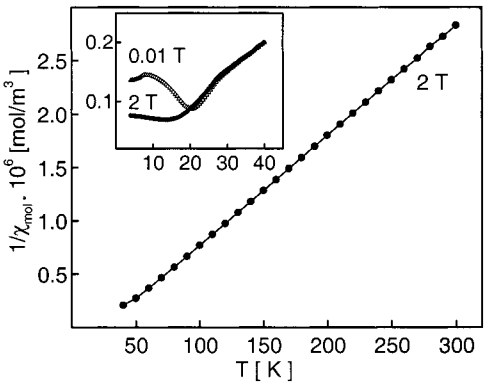


**Figure 29.** Temperature dependence of the inverse magnetic susceptibility of EuZnSn.

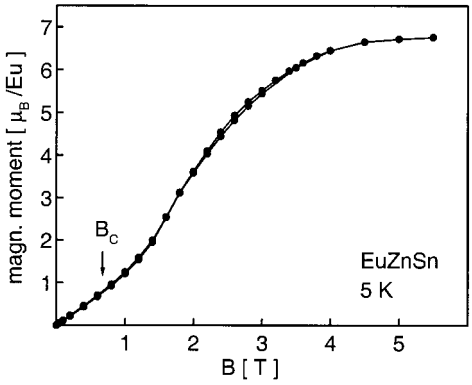


**Figure 30.** Magnetization vs external magnetic flux density of EuZnSn.

fields ($B_C$). As an example for a typical metamagnet we present the data of the Zintl phase EuZnSn.[117] This stannide orders antiferromagnetically at $T_N = 20.5(2)$ K (Figure 29) and a metamagnetic transition occurs at the small critical field of $B_C = 0.7(1)$ *T* (Figure 30). The saturation magnetization of $\mu_{sm(exp)} = 6.80(5)\ \mu_B$/Eu is close to the theoretical value of $\mu_{sm(calc)} = 7.0\ \mu_B$/Eu (calculated from $\mu_{sm(calc)} = g \times J$).[3] A spin-flop transition was observed for EuLiBi.[118]

Several of the EuTX compounds order ferromagnetically. The highest Curie temperatures of $T_C = 36$ and 38 K were observed for the gallides EuPtGa and EuPdGa,[125] respectively. An interesting ferromagnet is the germanide EuAuGe.[62,120] The EuAuGe structure contains two crystallographically independent europium sites.[62] One of these sites orders ferromagnetically at $T_C = 32.9(2)$ K and the second transition is detected at 18 K, in agreement with $^{151}$Eu Mössbauer spectroscopic results.[120] The magnetization curves of these ferromagnets show only small remanent magnetizations, small coercitive field strengths, and very narrow hystereses loops, classifying these compounds as soft ferromagnets.

EuZnGa[25] and EuAgGe[59] crystallize with the $KHg_2$ type with a statistical distribution of the Zn(Ag) and Ga(Ge) atoms on the mercury site (see chapters 3.2. and 3.5.). This structural disorder is also nicely reflected in the magnetic properties. EuAgGe and EuZnGa behave like spin glasses. Because of the statistical occupancies no magnetic long-range ordering is possible.

The magnetic properties of EuPtGe, EuAgSn, EuPdSn, EuPdSi, and EuPdIn have been investigated by different groups (Table 10); however, these results were essentially identical. Discrepancies occurred for the

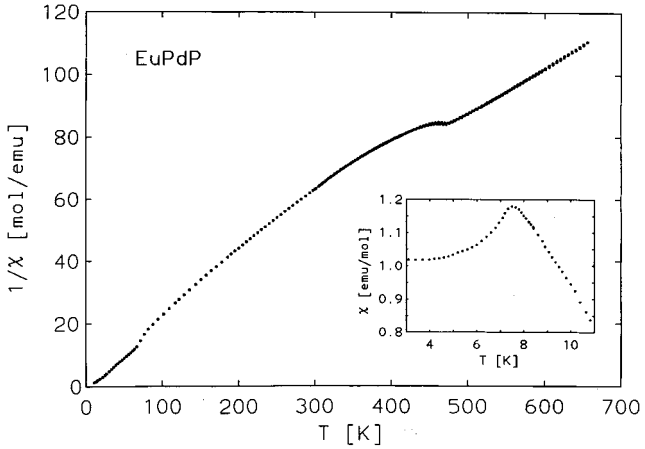


**Figure 31.** Temperature dependence of the inverse susceptibility of EuPdP.[91] The low-temperature susceptibility is shown in the insert.

susceptibility data of EuAuGa. While no magnetic ordering has been observed by Malik et al.,[124] ferromagnetic ordering at $T_C = 16(1)$ K has recently been detected during a reinvestigation.[121]

The physical properties of the equiatomic pnictides have most intensively been investigated. First magnetic susceptibility measurements of those compounds with the coin metals as transition metal component were carried out by Tomuschat and Schuster.[13] Some years later, the pnictides were investigated in more detail.

In 1991, the properties of EuPtP[85] were first studied.[89,130] EuPtP shows a strong temperature dependence of the magnetic susceptibility and undergoes two first-order phase transitions at 235 and 190 K. These phase transitions are also characterized by discontinuities in the lattice parameters and in the magnetic susceptibility.[130] At low temperatures EuPtP shows two inequivalent europium sites. Both of these sites have an occupancy of 50%. Antiferromagnetic ordering at 8.6 K is observed for one site which is close to divalent europium.

A similar behavior was also observed for EuNiP, EuPdP,[91] and EuPdAs.[91,127] The valence changes in these compounds by about $^1/_6$ at the phase transition, thus resulting in mean europium valences of $2n/6$. This peculiar behavior can be explained in a model of charged layers[91,130] where the effective charge is increased with increasing europium valence. The factor of $n/6$ most likely results from the hexagonal europium environment for each europium atom within the planes (Figure 16). As an example for the magnetic behavior we present the inverse susceptibility of EuPdP in Figure 31. Since the physical properties of the whole series of the mixed-valent pnictides have been reviewed recently competently by Michels et al.,[91] we only give a brief summary here.

*5.2.2. Mössbauer Spectroscopy.* Two different Mössbauer nuclei have been used for the study of magnetic hyperfine interactions in the equiatomic europium compounds: $^{151}$Eu to study the europium valence and $^{119}$Sn to search for transferred magnetic hyperfine fields. $^{151}$Eu Mössbauer spectroscopy is the most useful tool to distinguish between inhomogeneously (quasi-static) mixed valence (two separated lines at ~0 mm/s and ~ −10 mm/s) and intermediate (fluctuating) valence (one line at an intermediate position). The absence of a

**Table 12. $^{151}$Eu Mössbauer Spectroscopic Data of Ternary EuTX Compounds[a]**

| compd | $T$ [K] | $\delta$ [mm/s] | $T_O$ [K] | $\Gamma$ [mm/s] | $\Delta E_Q$ [mm/s] | $B$ [T] | ref(s) |
|---|---|---|---|---|---|---|---|
| | | | | Gallides | | | |
| EuCuGa | 4.2 | −9.1 | | | | 21.2 | 124 |
| EuPdGa | 4.2 | −8.6 | | | | 22.6 | 125 |
| EuAgGa | 4.2 | −9.8 | | | | 18.2 | 124 |
| EuPtGa | 4.2 | −8.05 | | | | 28.0 | 125 |
| EuAuGa | 4.2 | −9.4 | | | | 25 | 124 |
| | | | | Indides | | | |
| EuZnIn | 4.2 | −10.27(9) | 9 | 3.8(3) | 5 | 20.1(3) | 123 |
| EuRhIn | 4.2 | −7.9(1) | 30 | 2.4 | 8(1) | 22.6(2) | 34 |
| EuPdIn | 4.2 | −8.8(1) | 15 | 2.4(1) | −2(1) | 22.2(1) | 123 |
| EuPtIn | 4.2 | −8.66 | 20 | 2.3 | 10(1) | 23.1(2) | 123 |
| EuAuIn | 4.2 | −9.7(4) | 20 | 2.3 | 8(1) | 21.5(2) | 123 |
| | | | | Silicides | | | |
| EuPdSi | 4.2 | −9.67 | | | | | 41 |
| EuPtSi | 4.2 | −9.85 | | | | | 41 |
| | | | | Germanides | | | |
| EuCuGe[b] | 4.2 | −9.8(1) | 20.5(5) | 2.6 | −6.9 | 27.7(5) | 134 |
| EuZnGe[b] | 4.2 | −10.9(1) | 18.5(5) | 2.5 | −2 | 25.5(7) | 134 |
| EuPdGe | 4.2 | −9.7(2) | 10 | 3.4(5) | | 20.7(5) | 128 |
| EuAgGe | 4.2 | −10.34(8) | 15(1) | 2.3 | | 26.0(6) | 120 |
| EuPtGe | 4.2 | −10.40(5) | | | 4(1) | | 12 |
| EuAuGe | 4.2 | −10.0(3) | 32 | 2.6 | | 21.3; 17.4 | 120 |
| | | | | Stannides | | | |
| EuCuSn | 4.2 | −10.17(1) | 11 | 2.3 | −3.2 | 23.1 | 129 |
| EuZnSn | 4.2 | −10.76(5) | 26 | 2.3 | | 23.4(1) | 117 |
| EuAgSn | 4.2 | −10.9(1) | 6 | 2.3 | 7.4 | 21.5 | 129 |
| EuAgSn | 4.2 | −11.0 | 7 | 3.5 | | 20 | 74 |
| EuPdSn | 4.2 | −9.57(5) | 21 | 2.5 | −5.1 | 22.2 | 129 |
| EuPtSn | 4.2 | −9.07(8) | 28 | 2.5 | −7 | 28.2 | 129 |
| EuAuSn | 4.2 | −10.88(9) | 12 | 3.5(4) | | 21.4; 10.3; 2.2 | 77 |
| | | | | Plumbides | | | |
| EuAuPb | 4.2 | −10.9 | 8 | | | | 82 |
| | | | | Phosphides | | | |
| EuNiP | 300 | 0.06(6) | | 2.6 | | | 91 |
| | | −9.32(1) | | 3.3 | | | |
| EuCuP | 300 | −10.83 | | 2.86 | | | 126 |
| EuPdP | 300 | −0.60(4) | | 2.9 | | | 91 |
| | | −10.22(5) | | 3.5 | | | |
| EuPtP | 300 | −9.41 | | 3.19 | | | 91 |
| | 235 | −9.41 | | | | | |
| | | −1.06 | | | | | |
| | 11 | −10.30 | | | | | |
| | | −0.35 | | | | | |
| EuAuP | 300 | −11.56(3) | | 2.61 | | | 126 |
| EuLiP | 4.2 | −10.6 | | 2.3 | 2.8 | 25.8 | 88, 132 |
| | | | | Arsenides | | | |
| EuPdAs | 197 | −10.3 | | | 1.3 | | 127 |
| | 197 | +0.5 | | | 1.0 | | 127 |
| | 10 | −10.7 | | | 1.3 | | 127 |
| | 10 | −0.6 | | | 1.0 | | 127 |
| EuLiAs | 4.2 | −10.9 | | 2.3 | 0.3 | 22.7 | 88, 132 |
| | | | | Antimonides | | | |
| EuLiSb | 4.2 | −11.4 | | 2.3 | 2.1 | 18.2 | 88, 132 |
| | | | | Bismuthides | | | |
| EuLiBi | 4.2 | −11.3 | | 2.3 | −1.8 | 20.2 | 88, 132 |

[a] Abbreviations: $T$, temperature of the measurement; $\delta$, isomer shift; $T_O$, Mössbauer ordering temperature; $\Gamma$, experimental line width; $\Delta E_Q$, quadrupole splitting parameter; $B$, hyperfine field at the europium nucleus. [b] These compounds show no full magnetic hyperfine field splitting down to 4.2 K. Ordering parameters of 0.75 (EuCuGe), respectively 0.73 (EuZnGe) and fluctuation frequencies were applied in the refinements.

(trivalent) Mössbauer line around 0 mm/s clearly excludes an inhomogeneously mixed-valent state.

Although many $^{151}$Eu Mössbauer data of the EuTX compounds are available, these investigations have not been carried out as extensively as the magnetic characterizations. The results of the $^{151}$Eu Mössbauer experiments are listed in Table 12. In agreement with the magnetic data, most EuTX compounds show isomer shifts of about −10 mm/s. Within the whole family of EuTX compounds the isomer shifts cover the large range from −7.9 mm/s (EuRhIn) to −10.9 mm/s (EuAuPb), depending on the electronic structure of the respective material, i.e., the s electron density at the europium nuclei. Similar ranges of the isomer shift have also been observed for the series of pnictides (Table 12).

Below the magnetic ordering temperatures, the $^{151}$Eu Mössbauer spectra show magnetic hyperfine field splitting with magnetic hyperfine fields up to 28 T at the europium nuclei. As an example, we present the 4.2 K spectrum of EuRhIn (TiNiSi type) in Figure 32.[34] An

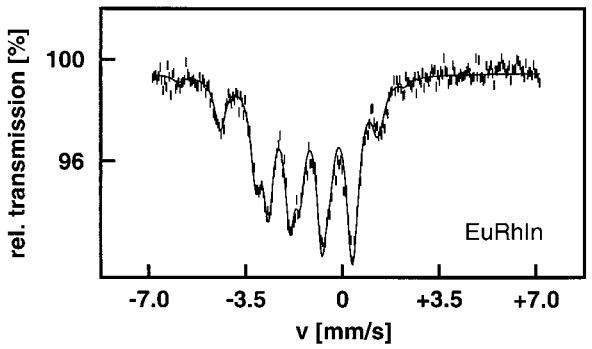


**Figure 32.** $^{151}$Eu Mössbauer spectrum of EuRhIn at 4.2 K.

interesting correlation of the $^{151}$Eu isomer shifts with the shortest Eu−Eu distances within the zigzag chains of the $KHg_2$ respectively TiNiSi type structures was recently observed for the series EuRhIn, EuPtIn, EuPdIn, EuAuIn, and EuZnIn, where the isomer shift linearly increases with decreasing Eu−Eu distances.[34,123]

The $^{151}$Eu Mössbauer spectra of the coin metal pnictides Eu(Cu,Ag,Au)(P,As,Sb) are compatible with nearly divalent europium[126] in agreement with the magnetic properties investigated earlier.[13,119] The experimental magnetic moments of these pnictides range between 7.45 and 7.72 $\mu_B$/Eu,[13,119] sligthly lower than the calculated value of 7.94 $\mu_B$/Eu for the free $Eu^{2+}$ ion [3]. $L_{III}$ X-ray absorption spectra (see below) indicate nonintegral valences (2.13−2.22), most likely resulting from final-state effects.

According to temperature-dependent $^{151}$Eu Mössbauer spectra, static mixed valence occurs in EuNiP and EuPdP with different $Eu^{2+}/Eu^{3+}$ contributions. A homogeneous mixed-valence is observed in EuPtP above 235 K,[91] whereas quasistatic behavior is observed below this temperature. As an example the $^{151}$Eu Mössbauer spectrum of EuNiP is shown in Figure 33,[135] heating from room temperature to 473 K, a continuous transition from quasi-static (two lines) to inhomogeneous mixed valence (one line) is clearly shown. The $^{151}$Eu Mössbauer spectra of mixed-valent EuPdAs reveal a fluctuation between $Eu^{2+}$ and $Eu^{3+}$ slower than $10^8$ Hz, i.e., the europium ions are quasi-static. Thus, two independent Mössbauer signals at $\delta_I = -10.3$ mm/s and $\delta_{II} = +0.5$ mm/s occur in the Mössbauer spectra below 200 K.[127] This behavior is very similar to EuPtP.[85,91]

The series of EuTSn stannides has been investigated by $^{151}$Eu and $^{119}$Sn Mössbauer spectroscopy.[74,77,117,129] These stannides show transferred magnetic hyperfine fields at the tin nuclei below the magnetic ordering temperature of the europium atoms. Nevertheless, in most stannides the transferred hyperfine fields are small, leading to significant line broadening of the spectra. This is different in the Zintl phase EuZnSn,[117] where a transferred hyperfine field of 12.8 T was detected at the tin site (Figure 34), leading to a symmetrically split spectrum.

*5.2.3. Electrical Conductivity.* The transport properties have been investigated for several EuTX compounds. According to electronic structure calculations (see chapter 4), most EuTX compounds can be considered as metallic Zintl phases. Up to now, all resistivity measurements revealed metallic behavior over the temperature ranges investigated. As an example we present the resistivity of EuZnGe in Figure 35. The

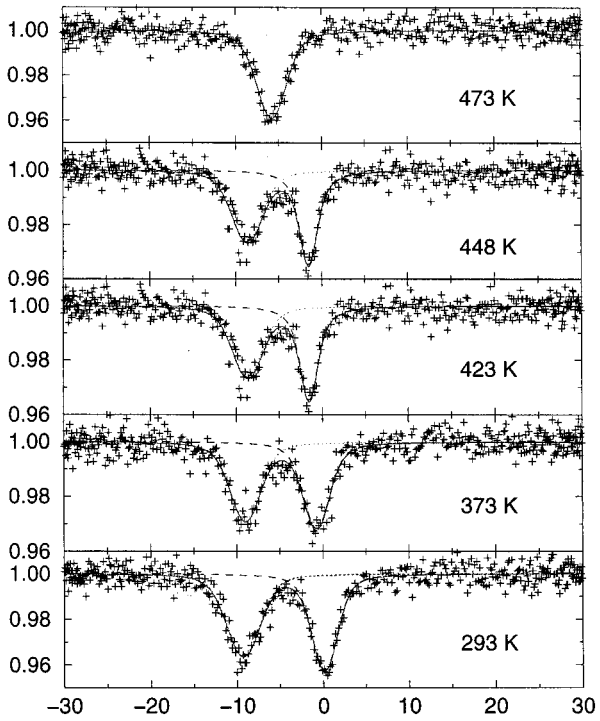


**Figure 33.** $^{151}$Eu Mössbauer spectra of EuNiP at different temperatures.

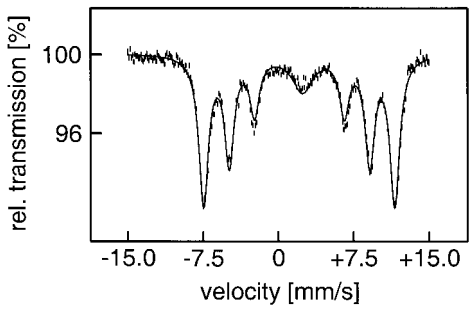


**Figure 34.** $^{119}$Sn Mössbauer spectrum of EuZnSn at 4.2 K.

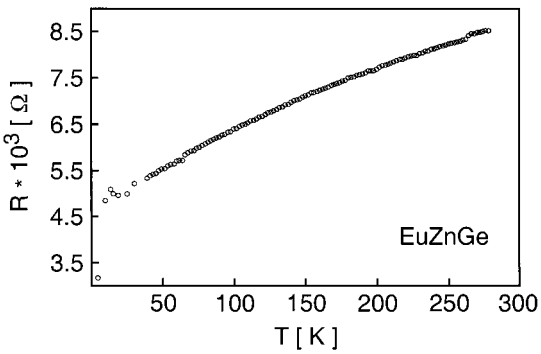


**Figure 35.** Temperature dependence of the electrical resistivity of EuZnGe.

room-temperature specific resistivities of the EuTX compounds cover the range from 20 to 500 $\mu\Omega$cm. According to these values these compounds can be classified as reasonably good metallic conductors. In most cases, however, the irregular shaped character and grain boundaries of the polycrystalline samples avoided the determination of absolute values, as it is also the case for EuZnGe.

Several of the EuTX compounds show anomalies in the specific resistivity at low temperature which arises

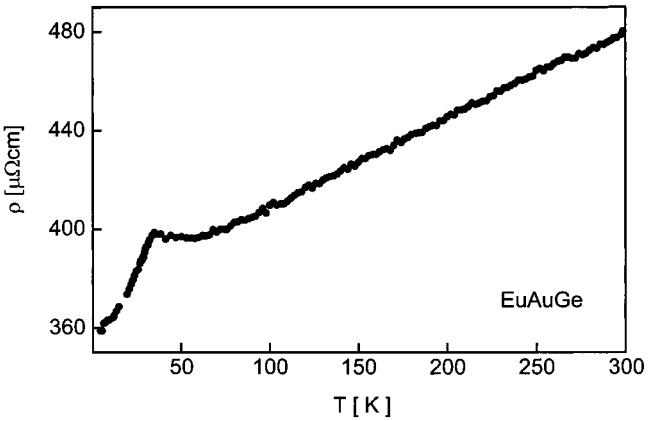


**Figure 36.** Temperature dependence of the specific resistivity of EuAuGe.

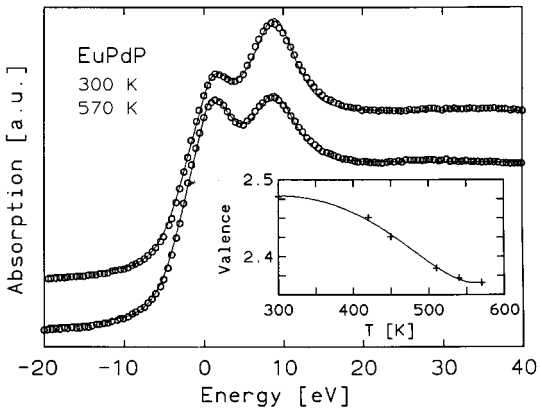


**Figure 37.** $L_{III}$ X-ray absorption spectrum of EuPdP at 300 and 570 K.[91] The temperature dependence of the mean valence is shown in the insert.

from a decrease of spin-disorder scattering in the magnetically ordered state. A striking example is the 32.9 K ferromagnet EuAuGe.[62] The specific resistivity of this germanide shows a sharp drop at the Curie temperature (Figure 36).

Also the mixed-valent pnictides EuPtP[131] and EuPdAs[127] show a strong temperature dependence of the resistivity at the transition temperatures. Above and below the transition temperatures the resistivity of EuPtP single crystals and polycrystalline EuPdAs pieces is of metallic type, while a giant increase occurs in the region of the phase transition. Point-contact experiments of EuPtP single crystals with platinum and molybdenum needles show structures related to the two magnetic ordering temperatures.

In spin glass systems such as EuAgGe[120] no pronounced anomaly occurs down to 4.2 K. Nevertheless, broad minima can be observed at low temperatures, most likely due to magnetic scattering at the cluster glass (mictomagnet).

*5.2.4. $L_{III}$ Spectra and Resonant Photoemission.* Energy dispersive $L_{III}$ absorption spectra (XAS) have been measured for only a few of the EuTX compounds, mostly the pnictides. These measurements result in values for the mean europium valence and are thus a complementary method to $^{151}$Eu Mössbauer spectroscopy. Nevertheless, some words of caution seem to be appropriate at this point. XAS measurements are a surface-sensitive method and any surface oxidation ($Eu^{2+} \rightarrow Eu^{3+}$) of the material can affect the spectra.

EuPtP shows a double-peaked structure, indicating the existence of divalent and trivalent europium in the sample. According to the $L_{III}$ spectra, the mean europium valence increases from 2.18 to 2.40 from room temperature down to 4 K.[91] Similar results were obtained for EuNiP and EuPdP. As an example we present $L_{III}$ spectra of mixed-valent EuPdP in Figure 37. With regard to the remaining EuTX compounds, only EuScGe[53,64] was investigated by $L_{III}$ spectra, indicating divalent europium in this germanide.

The europium valence in EuPdP, EuAuAs, and EuAgP was also studied by photoemission experiments.[101−103] The experimentally determined 4f density-of-states at the Fermi level have been compared with results from TB-LMTO-ASA band structure calculations. These investigations unambiguously showed that in the case of divalent europium compounds, i.e., EuAuAs, the conduction band has mainly Eu d character, while a high density of 4f states close to the Fermi level is observed in the photoemission measurements for EuPdP. Furthermore, the TB-LMTO-ASA band structure calculations for EuPdP reveal a van Hove singularity close to the Fermi level, indicating that a high 4f density-of-states at $E_F$ is only one necessary condition for dynamic valence fluctuations.

Substitution experiments in the series $EuPd_{1-x}Ag_xP$ and $EuPd_{1-x}Au_xP$[101] showed a drastic change in the lattice parameters. These anomalies are mainly due to electronic factors (filling of antibonding levels) and changes of the valence of the europium atoms at the same time. However, the valence instabilities are limited to a small ranges of VEC near the pure palladium compounds, i.e., $x < 0.4$ for Ag and $x < 0.5$ for Au.

*5.2.5. High-Pressure Investigations.* EuPdGe and EuPdSi have intensively been investigated under high-pressure conditions.[44] Monoclinic NP−EuPdGe[44,58] with EuNiGe type structure transforms at 4 GPa and 1270 K to orthorhombic HP-EuPdGe with TiNiSi type. The coordination of the palladium atoms increases from three to four. Cubic EuPdSi with LaIrSi type structure transforms at 4 GPa and 1120 K into a two-phased sample: about 80% $EuPd_{1.33}Si_{0.67}$ with $MgZn_2$ structure and about 20% $EuPd_{0.56}Si_{1.44}$ with $AlB_2$ type.

The lattice parameters and compressibilities of the pnictides EuNiP, EuPdP, EuPtP, and EuPdAs have also been studied under high-pressure conditions, indicating extremely anisotropic changes of the lattice parameters which are accompanied by valence changes of the europium atoms.[92]

These few high-pressure investigations have so far only focused on the crystal chemistry. Most of the EuTX compounds show stable divalent europium at normal pressure conditions. It is highly probable, that the europium atoms loose their third valence electron under high-pressure conditions. This may result in interesting structural transitions and/or valence changes. Investigations of the EuTX compounds under high-pressure conditions are thus a very prospective domain for the experimental chemist.

## 6. Conclusion

In a nutshell, the rich crystal chemistry of a total of 72 equiatomic EuTX compounds which crystallize in 12

different structure types has been reviewed. The T components are transition metals from the cobalt to the copper group and X is an element of the III, IV, or V main group. The electron count of the respective EuTX compounds can effectively be varied through a substitution of the T and X components. The electronic structure of these materials was investigated by LMTO band structure calculations. Chemical bonding is governed by strong covalent T−X interactions within the polyanions and rather ionic Eu−T(X) bonds.

Additionally the greatly varying magnetic and electrical properties are reviewed. Besides simple paramagnets, antiferro- or ferromagnetic ground states occur. Some EuTX compounds show spin-glass behavior and several of the pnictides are characterized as intermediate-valence systems. The magnetic investigations have been paralleled by $^{151}$Eu Mössbauer spectroscopy and $L_{III}$ X-ray absorption experiments to investigate the valence behavior of the europium atoms in more detail. The X-ray crystallographic results together with physical property measurements have enabled to figure out structure−property relations for several compounds.

Although numerous investigations of EuTX compounds have been performed, this peculiar family of intermetallics still has a large potential for further studies. A fruitful future strategy might certainly be the examination of the structures and properties under high-pressure conditions.

**Acknowledgment.** We thank Professors Eckert, Jeitschko, Mewis, and Simon for their interest and steady support of this work. We are also indebted to our co-workers and collegues mentioned in the various references for experimental help and fruitful discussions. Special thanks go to Dr. W. Gerhartz (Degussa AG) and Dr. G. Höfer (Heraeus Quarzschmelze) for generous gifts of platinum metals and silica tubes. This work was financially supported by the Deutsche Forschungsgemeinschaft and the Fonds der Chemischen Industrie.

## References

(1) Villars, P.; Calvert, L. D. *Pearson's Handbook of Crystallographic Data for Intermetallic Compounds*; American Society for Metals: Materials Park, OH 44073; 2nd ed., 1991, and desk edition, 1997.
(2) Parthé, E.; Chabot, B. Crystal structures and crystal chemistry of ternary rare earth transition metal borides, silicides and homologues. In *Handbook on the Physics and Chemistry of Rare Earths*; Gschneidner, K. A., Jr., Eyring, L., Eds.; ; Elsevier: New York, 1984; Chapter 48
(3) Szytuła, A.; Leciejewicz, J. *Handbook of Crystal Structures and Magnetic Properties of Rare Earth Intermetallics*; CRC Press: Boca Raton, FL, 1994.
(4) Fornasini, M. L.; Merlo, F. *J. Alloys Compd.* **1995**, *219*, 63.
(5) Fujita, T.; Suzuki, T.; Nishigori, S.; Takabatake, T.; Fujii, H.; Sakurai, J. *J. Magn. Magn. Mater.* **1992**, *108*, 35.
(6) McWhan, D. B.; Souers, P. C.; Jura, G. *Phys. Rev.* **1966**, *143*, 385.
(7) Stroka, B.; Wosnitza, J.; Scheer, E.; Löhneysen, H. v.; Park, W.; Fischer, K. *Z. Phys. Condens. Matter* **1992**, *89*, 39.
(8) Krauss, H. L.; Stach, H. *Z. Anorg. Allg. Chem.* **1969**, *366*, 34.
(9) Schenk, P. W.; Steudel, R.; Brauer, G. Teil I, Präparative Methoden. In Brauer, G. *Handbuch der Präparativen Anorganischen Chemie*; Enke, F., Ed.; Stuttgart, 1975.
(10) Busch, G.; Kaldis, E.; Muheim, J.; Bischof, R. *J. Less-Common Met.* **1971**, *24*, 453.
(11) Spedding, F. H.; Beaudry, B. J.; Croat, J. J.; Palmer, P. E. *Proc. Inter Am. Conf. Mater. Technol., San Antonio, Texas, May 20−24* **1968**, 151.
(12) Pöttgen, R.; Kremer, R. K.; Schnelle, W.; Müllmann, R.; Mosel, B. D. *J. Mater. Chem.* **1996**, *6*, 635.
(13) Tomuschat, C.; Schuster, H.-U. *Z. Naturforsch.* **1981**, *36b*, 1193.
(14) Johrendt, D.; Mewis, A. *J. Alloys Compd.* **1992**, *183*, 210.
(15) Corbett, J. D. *Inorg. Synth.* **1983**, *22*, 15.
(16) Pöttgen, R.; Gulden, Th.; Simon, A. *GIT Labor-Fachzeitschrift* **1999**, *43*, 133.
(17) Pöttgen, R.; Lang, A.; Hoffmann, R.-D.; Müllmann, R.; Mosel, B. D.; Künnen, B.; Kotzyba, G. *Z. Kristallogr.* **1999**, *214*, 143.
(18) Kussmann, D.; Hoffmann, R.-D.; Pöttgen, R. *Z. Anorg. Allg. Chem.* **1998**, *624*, 1727.
(19) Hulliger, F. *J. Alloys Compd.* **1993**, *200*, 75.
(20) Shoemaker, C. B.; Shoemaker, D. P. *Acta Crystallogr.* **1965**, *18*, 900.
(21) Iandelli, A. *J. Less-Common Met.* **1987**, *135*, 195.
(22) Dwight, A. E. *J. Less-Common Met.* **1987**, *127*, 175.
(23) Duwell, E. J.; Baenziger, N. C. *Acta Crystallogr.* **1955**, *8*, 705.
(24) Pöttgen, R.; Grin, Y. *Z. Kristallogr.* **1996**, *Suppl. 11*, 93.
(25) Pöttgen, R.; Grin, Y. *Z. Kristallogr.* **1997**, *Suppl. 12*, 137.
(26) Larson, A. C.; Cromer, D. T. *Acta Crystallogr.* **1961**, *14*, 73.
(27) Parthé, E.; Gelato, L. M. *Acta Crystallogr.* **1984**, *A40*, 169.
(28) Pöttgen, R.; Hoffmann, R.-D.; Grin, Y. *Z. Kristallogr.* **1999**, Suppl. 16, 55.
(29) Pöttgen, R.; Grin, Y. Unpublished results.
(30) Ferro, R.; Marazza, R.; Rambaldi, G. *Z. Metallkd.* **1974**, *65*, 37.
(31) Cirafici, S.; Palenzona, A.; Canepa, F. *J. Less-Common Met.* **1985**, *107*, 179.
(32) Pöttgen, R. *J. Mater. Chem.* **1996**, *6*, 63.
(33) Pauling, L. *The Nature of the Chemical Bond and the Structure of Molecules and Crystals*; Cornell University Press: Ithaca, NY, 1960.
(34) Pöttgen, R.; Hoffmann, R.-D.; Möller, M. H.; Kotzyba, G.; Künnen, B.; Rosenhahn, C.; Mosel, B. D. *J. Solid State Chem.* **1999**, *145*, 174.
(35) Pöttgen, R. *Z. Kristallogr.* **1996**, *211*, 884.
(36) Pöttgen, R. Unpublished results.
(37) Zarechnjuk, O. S.; Janson, T. I. *Dopov. Akad. Nauk Ukr. RSR, Ser. B* **1982**, 30.
(38) Merlo, F.; Pani, M.; Fornasini, M. L. *J. Less-Common Met.* **1991**, *171*, 329.
(39) Merlo, F.; Pani, M.; Fornasini, M. L. *J. Alloys Compd.* **1993**, *196*, 145.
(40) Evers, J.; Oehlinger, G.; Polborn, K.; Sendlinger, B. *J. Solid State Chem.* **1991**, *91*, 250.
(41) Adroja, D. T.; Padalia, B. D.; Malik, S. K.; Nagarajan, R.; Vijayaraghavan, R. *J. Magn. Magn. Mater.* **1990**, *89*, 375.
(42) Merlo, F.; Pani, M.; Fornasini, M. L. *J. Alloys Compd.* **1996**, *232*, 289.
(43) Evers, J.; Oehlinger, G. *J. Solid State Chem.* **1986**, *62*, 133.
(44) Sendlinger, B. Hochdruck-Untersuchungen an den ambivalenten Verbindungen MTX (M = Yb, Ca, Eu, Sr, Ba; T = Pd, Pt; X = Si, Ge, Sn, Pb). Dissertation, Ludwig-Maximilians-Universität, München, 1993.
(45) Gil, R. C.; Carrillo-Cabrera, W.; Schultheiss, M.; Peters, K.; von Schnering, H. G. *Z. Anorg. Allg. Chem.* **1999**, *625*, 285.
(46) Klepp, K.; Parthé, E. *Acta Crystallogr. Sect. B* **1982**, *38*, 1541.
(47) Janzon, K. H.; Schäfer, H.; Weiss, A. *Angew. Chem.* **1965**, *77*, 258.
(48) Krypyakevich, P. I.; Gladyshevskii, E. I. *Sov. Phys. Crystallogr.* **1966**, *11*, 693.
(49) Pringle, G. E. *Acta Crystallogr. Sect. B* **1972**, *28*, 2326.
(50) Zhao, J. T.; Parthé, E. *Acta Crystallogr. Sect. C* **1990**, *46*, 2276.
(51) Brauer, G.; Mitius, A. *Z. Anorg. Allg. Chem.* **1942**, *249*, 325.
(52) Klepp, K.; Parthé, E. *Acta Crystallogr. Sect. B* **1982**, *38*, 1105.
(53) Bodak, O. I.; Kokhan, Z. M. *Inorg. Mater.* **1983**, *19*, 987.
(54) Oniskovets, B. D.; Bel'skii, V. K.; Pecharskii, V. K.; Bodak, O. I. *Sov. Phys. Crystallogr.* **1987**, *32*, 522.
(55) Pöttgen, R. Präparative, kristallchemische und magnetische Untersuchungen an binären und ternären intermetallischen Europiumverbindungen mit einem Beitrag über Verwachsungsstrukturen in intermetallischen Verbindungen. Habilitationsschrift, Universität Münster, 1996.
(56) Iandelli, A. *J. Alloys Compd.* **1993**, *198*, 141.
(57) Pöttgen, R. *Z. Kristallogr.* **1995**, *210*, 924.
(58) Pöttgen, R. *Z. Naturforsch.* **1995**, *50b*, 1181.
(59) Pöttgen, R. *Z. Naturforsch.* **1995**, *50b*, 1071.
(60) Evers, J.; Oehlinger, G.; Polborn, K.; Sendlinger, B. *J. Less-Common Met.* **1992**, *182*, L23.
(61) Zmii, O. F.; Gladyshevskii, E. I. *Sov. Phys. Crystallogr.* **1971**, *15*, 817.
(62) Pöttgen, R. *J. Mater. Chem.* **1995**, *5*, 505.
(63) Stassen, W. N.; Sato, M.; Calvert, L. D. *Acta Crystallogr. Sect. B* **1970**, *26*, 1534.
(64) Bodak, O. I.; Shpyrka, Z. M.; Mokra, I. R. *J. Alloys Compd.* **1997**, *247*, 217.
(65) Donohue, J. *The Structures of the Elements*; Wiley: New York, 1974.
(66) Siegrist, T.; Hulliger, F. *J. Solid State Chem.* **1986**, *63*, 23.
(67) Yarmolyuk, Ya. P.; Grin, Yu. N.; Vasilechko, L. O.; Bel'skii, V. K. *Sov. Phys. Crystallogr.* **1986**, *31*, 106.

(68) Dörrscheidt, W.; Niess, N.; Schäfer, H. *Z. Naturforsch.* **1977**, *32b*, 985.
(69) Kussmann, D.; Hoffmann, R.-D.; Pöttgen, R. *Z. Kristallogr.* **1998**, *Suppl. 15*, 52.
(70) Details concerning the structure refinement may be obtained from: FIZ-Karlsruhe, D-76344 Eggenstein-Leopoldshafen, by quoting the regisry number CSD-411034. E-mail: crysdata@fiz-karlsruhe.de.
(71) Wörle, M.; Nesper, R.; Mair, G.; Schwarz, M.; von Schnering, H. G. *Z. Anorg. Allg. Chem.* **1995**, *621*, 1153.
(72) Zachwieja, U. *Z. Anorg. Allg. Chem.* **1996**, *622*, 1173.
(73) Pöttgen, R. *J. Alloys Compd.* **1996**, *243*, L1.
(74) Hossain, Z.; Nagarajan, R.; Etilé, M.; Godart, C.; Kappler, J. P.; Gupta, L. C.; Vijayaraghavan, R. *J. Magn. Magn. Mater.* **1995**, *150*, 223.
(75) Adroja, D. T.; Malik, S. K. *Phys. Rev.* **1992**, *45B*, 779.
(76) Pöttgen, R. *Z. Naturforsch.* **1996**, *51b*, 806.
(77) Pöttgen, R.; Hoffmann, R.-D.; Müllmann, R.; Mosel, B. D.; Kotzyba, G. *Chem. Eur. J.* **1997**, *3*, 1852.
(78) Nuspl, G.; Polborn, K.; Evers, J.; Landrum, G. A.; Hoffmann, R. *Inorg. Chem.* **1996**, *35*, 6922.
(79) Iandelli, A. *Z. Anorg. Allg. Chem.* **1964**, *330*, 221.
(80) Pöttgen, R.; Borrmann, H.; Felser, C.; Jepsen, O.; Henn, R.; Kremer, R. K.; Simon, A. *J. Alloys Compd.* **1996**, *235*, 170.
(81) Pöttgen, R.; Kotzyba, G. *J. Alloys Compd.* **1996**, *245*, L9.
(82) Arpe, P. E. Synthese und strukturchemische Untersuchungen an ternären Plumbiden des Ytterbiums. Staatsexamensarbeit. Universität Münster, 1997.
(83) Keimes, V. Kristallstrukturen ternärer Pnictide mit unedlen zwei- oder dreiwertigen Metallen. Dissertation, Universität zu Köln, 1993.
(84) Johrendt, D. Ternäre Palladiumverbindungen mit Elementen der 5. Hauptgruppe und Untersuchungen in den Systemen Seltenerdmetall-Aluminium−Germanium. Dissertation, Universität zu Köln, 1993.
(85) Lux, C.; Mewis, A.; Lossau, N.; Michels, G.; Schlabitz, W. *Z. Anorg. Allg. Chem.* **1991**, *593*, 169.
(86) Lux, C.; Mewis, A.; Junk, S.; Gruetz, A.; Michels, G. *J. Alloys Compd.* **1993**, *200*, 135.
(87) Albering, J. H.; Ebel, Th.; Jeitschko, W. *Z. Kristallogr.* **1997**, *Suppl. 12*, 242.
(88) Albering, J. H. Struktur und Eigenschaften ternärer Actinoid-Übergangsmetall-Phosphide und ähnlicher Verbindungen. Dissertation. Universität Münster, 1994.
(89) Lossau, N.; Kierspel, H.; Langen, J.; Schlabitz, W.; Wohlleben, D.; Sauer, Ch. *Z. Phys. B* **1989**, *74*, 227.
(90) Michels, G.; Huhnt, C.; Scharbrodt, W.; Holland-Moritz, E.; Johrendt, D.; Mewis, A.; Schlabitz, W. *Physica B* **1994**, *199/200*, 612.
(91) Michels, G.; Huhnt, C.; Scharbrodt, W.; Schlabitz, W.; Holland-Moritz, E.; Abd-Elmeguid, M. M.; Micklitz, H.; Johrendt, D.; Keimes, V.; Mewis, A. *Z. Phys. B* **1995**, *98*, 75.
(92) Huhnt, C.; Michels, G.; Schlabitz, W.; Johrendt, D.; Mewis, A. *J. Phys. C* **1997**, *9*, 9953.
(93) Mewis, A. *Z. Naturforsch.* **1978**, *33b*, 983.
(94) Wenski, G.; Mewis, A. *Z. Anorg. Allg. Chem.* **1986**, *543*, 49.
(95) Malik, S. K.; Adroja, D. T. *J. Magn. Magn. Mater.* **1991**, *102*, 42.
(96) Merlo, F.; Pani, M.; Fornasini, M. L. *J. Less-Common Met.* **1990**, *166*, 319.
(97) Bärnighausen, H. *Commun. Math. Chem.* **1980**, *9*, 139.
(98) Bärnighausen, H.; Müller, U. Symmetriebeziehungen zwischen den Raumgruppen als Hilfsmittel zur straffen Darstellung von Strukturzusammenhängen in der Kristallchemie. Universität Karlsruhe and Universität-Gh Kassel, Germany, 1996.
(99) Pöttgen, R.; Hoffmann, R.-D. *Z. Kristallogr.*, submitted for publication.
(100) Felser-Wenz, C. Bandstrukturechnungen und Photoemissionsexperimente an zwischenvalenten Europiumverbindungen. Dissertation, Universität zu Köln, 1995.
(101) Johrendt, D.; Felser, C.; Huhnt, C.; Michels, G.; Schäfer, W.; Mewis, A. *J. Alloys Compd.* **1997**, *241*, 21.
(102) Felser, C. *J. Alloys Compd.* **1997**, *262−263*, 87.
(103) Felser, C.; Cramm, S.; Johrendt, D.; Mewis, A.; Jepsen, O.; Hohlneicher, G.; Eberhardt, W.; Andersen, O. K. *Europhys. Lett.* **1997**, *40*, 85.
(104) Zheng, Ch.; Hoffmann, R. *Inorg. Chem.* **1989**, *28*, 1074.
(105) Burdett, J. K.; Miller, G. J. *Chem. Mater.* **1990**, *2*, 12.
(106) Johrendt, D.; Mewis, A. *Z. Naturforsch.* **1996**, *51b*, 655.
(107) Landrum, G. A.; Hoffmann, R.; Evers, J.; Boysen, H. *Inorg. Chem.* **1998**, *37*, 5754.
(108) Pearson, R. G. *Inorg. Chem.* **1988**, *27*, 734.
(109) Jepsen, O.; Snob, M.; Andersen, O. K. *Linearized Band-Structure Methods in Electronic Band-Structure and its Applications*; Springer Lecture Notes; Springer: Berlin, 1987.
(110) Dronskowski, R.; Blöchl, P. E. *J. Phys. Chem.* **1993**, *97*, 8617.
(111) Hughbanks, T.; Hoffmann, R. *J. Am. Chem. Soc.* **1983**, *105*, 3528.
(112) Schnelle, W.; Pöttgen, R.; Kremer, R. K.; Gmelin, E.; Jepsen, O. *J. Phys. C* **1997**, *9*, 1435.
(113) Gelato, L. M.; Parthé, E. *J. Appl. Crystallogr.* **1987**, *20*, 139.
(114) Silvi, B.; Savin, A. *Nature* **1994**, *371*, 683.
(115) Savin, A.; Nesper, R.; Wengert, S.; Fässler, T. F. *Angew. Chem.* **1997**, *109*, 1893.
(116) Fässler, Th. F.; Savin, A. *Chem. Unserer Zeit* **1997**, *31*, 110.
(117) Ernet, U.; Müllmann, R.; Mosel, B. D.; Eckert, H.; Pöttgen, R.; Kotzyba, G. *J. Mater. Chem.* **1997**, *7*, 255.
(118) Ebel, T. Magnetische Eigenschaften ternärer Uran- und Seltenerd-Übergangsmetall-Aluminide, -Carbide und -Phosphide und ähnlicher Verbindungen. Dissertation, Universität Münster, 1995.
(119) Tomuschat, C.; Schuster, H.-U. *Z. Anorg. Allg. Chem.* **1984**, *518*, 161.
(120) Müllmann, R.; Mosel, B. D.; Eckert, H.; Pöttgen, R.; Kremer, R. K. *Hyperfine Interact.* **1997**, *108*, 389.
(121) Grin, Yu.; Pöttgen, R.; Kremer, R. K. Unpublished results.
(122) Ito, T.; Nishigori, S.; Hiromitsu, I.; Kurisu, M. *J. Magn. Magn. Mater.* **1998**, *177−181*, 1079.
(123) Müllmann, R.; Mosel, B. D.; Eckert, H.; Kotzyba, G.; Pöttgen, R. *J. Solid State Chem.* **1998**, *137*, 174.
(124) Malik, S. K.; Nagarajan, R.; Adroja, D. T.; Dwight, A. E. In *Theoretical and experimental aspects of valence fluctuations and heavy fermions*; Gupta, L. C., Malik, S. K., Eds.; Plenum Publishing Corporation: New York, 1987.
(125) Malik, S. K.; Shenoy, G. K.; Paulose, P. L.; Nagarajan, R.; Dwight, A. E.; Vaishnava, P. P.; Kimball, C. W. *Hyperfine Interact.* **1987**, *34*, 377.
(126) Michels, G.; Junk, S.; Schlabitz, W.; Holland-Moritz, E.; Abd-Elmeguid, M. M.; Dünner, J.; Mewis, A. *J. Phys. − Condens. Matter* **1994**, *6*, 1769.
(127) Michels, G.; Junk, S.; Lossau, N.; Schlabitz, W.; Wohlleben, D.; Johrendt, D.; Mewis, A.; Sauer, Chr.; Woike, Th. *Z. Phys. B − Condens. Matter* **1992**, *86*, 53.
(128) Halet, J.-F.; Saillard, J.-Y.; Müllmann, R.; Rosenhahn, C.; Mosel, B. D.; Pöttgen, R.; Kotzyba, G. To be published.
(129) Müllmann, R.; Mosel, B. D.; Eckert, H.; Kremer, R. K.; Hoffmann, R.-D.; Pöttgen, R. *J. Solid State Chem.*, to be published.
(130) Lossau, N.; Kierspel, H.; Michels, G.; Oster, F.; Schlabitz, W.; Wohlleben, D.; Sauer, Chr.; Mewis, A. *Z. Phys. B − Condens. Matter* **1989**, *77*, 393.
(131) Nowack, A.; Klug, J.; Lossau, N.; Mewis, A. *Z. Phys. B − Condens. Matter* **1989**, *77*, 381.
(132) Prill, M. Mössbauer-spektroskopische Untersuchungen an ausgewählten ternären Eisen- und Europiumpnictiden. Dissertation, Universität Münster, 1994.
(133) Grin, Yu.; Pöttgen, R.; Kotzyba, G. Unpublished results.
(134) Müllmann, R. $^{151}$Eu-Mössbauerspektroskopische Untersuchungen an ternären Europium-Übergangsmetall-Germaniden und $EuNiIn_4$. Diplomarbeit, Universität Münster, 1995.
(135) Felser, C.; Waldeck, M.; Johrendt, D.; Mewis, A.; Ensling, J.; Gütlich, P. *Europhys. Lett.*, submitted for publication.

CM991183V